nature materials

SUPPLEMENTARY INFORMATION

DOI: 10.1038/NMAT4290

Size- and shape-dependent foreign body immune response to materials implanted in rodents and non-human primates

Omid Veiseh*[1,2,3], Joshua C. Doloff*[1,3], Minglin Ma*[1,3,4], Arturo J. Vegas[1,3], Hok Hei Tam[1,2], Andrew Bader[1,3], Jie Li[1,3], Erin Langan[1,3], Jeffrey Wyckoff[l], Whitney S. Loo[2], Siddharth Jhunjhunwala[1,3], Alan Chiu[1,3], Sean Siebert[1,3], Katherine Tang[1,3], Jennifer Hollister-Lock[5], Stephanie Aresta-Dasilva[1,3], Matthew Bochenek[6], Joshua Mendoza-Elias[6], Yong Wang[6], Merigeng Qi[6], Danya M. Lavin[1,3], Michael Chen[1,3], Nimit Dholakia[1,3], Raj Thakrar[1,3], Igor Lacík[7], Gordon C. Weir[5], Jose Oberholzer[6], Dale L. Greiner[8], Robert Langer[1,2,3,9,10,11], and Daniel G. Anderson[1,2,3,9,10,11#]

1. David H Koch Institute for Integrative Cancer Research, Massachusetts Institute of Technology, 500 Main Street, Cambridge, MA, 02139, USA
2. Department of Chemical Engineering, Massachusetts Institute of Technology, 77 Massachusetts Avenue, Cambridge, MA, 02139, USA
3. Department of Anesthesiology, Boston Children's Hospital, 300 Longwood Ave, Boston, MA 02115, USA
4. Current address: Biological and Environmental Engineering, Cornell University, Ithaca, NY 14853, USA
5. Section on Islet Cell and Regenerative Biology, Research Division, Joslin Diabetes Center, One Joslin Place, Boston, MA 02215, USA
6. Division of Transplantation, Department of Surgery, University of Illinois at Chicago, Chicago, IL
7. Department for Biomaterials Research, Polymer Institute of the Slovak Academy of Sciences, Dubravska cesta 9, 845 41 Bratislava, Slovakia.
8. Program in Molecular Medicine, University of Massachusetts Medical School, Worcester, MA 01605, USA
9. Division of Health Science Technology, Massachusetts Institute of Technology, 77 Massachusetts Avenue, Cambridge, MA, 02139, USA
10. Institute for Medical Engineering and Science, Massachusetts Institute of Technology, 77 Massachusetts Avenue, Cambridge, MA, 02139, USA
11. Harvard-MIT Division of Health Science and Technology, Massachusetts Institute of Technology, 77 Massachusetts Avenue, Cambridge, MA, 02139, USA
* Equal contributing authors
#email: dgander@mit.edu; Tel.: +1 617 258 6843; fax: +1 617 258 8827.

© 2015 Macmillan Publishers Limited. All rights reserved

DOI: 10.1038/NMAT4290

Supplemental Index of Sections

© 2015 Macmillan Publishers Limited. All rights reserved

1. Materials and Methods

a. Materials/Reagents

All chemicals were obtained from Sigma-Aldrich (St. Louis, MO) and cell culture reagents from Life Technologies (Grand Island, NY), unless otherwise noted. Antibodies: Alexa Fluor 488-conjugated anti-mouse CD68 (Cat. #137012, Clone FA-11) and Alexa Fluor 647-conjugated anti-mouse Ly-6G/Ly-6C (Gr-1) (Cat. #137012, Clone RB6-8C5) were purchased from BioLegend Inc. (San Diego, CA). Alexa Fluor 647-conjugated anti-mouse TGF beta1 (Cat. #bs-0103R-A647) was purchased from Bioss antibodies. Cy3-conjugated anti-mouse alpha smooth muscle actin antibody was purchased from Sigma Aldrich (St. Louis MO). Filamentous actin (F-actin)-specific Alexa Fluor 488-conjugated Phalloidin, and Newport Green were purchased from Life Technologies (Grand Island, NY). Glass spheres of medium (500 µm) and large size (2 mm) where purchased from Sigma Aldrich (St. Louis, MO). Stainless steel spheres of medium (500µm) and large (2.5mm) size were purchased from Thomas Scientific (Swedesboro, NJ). Polystyrene spheres of medium (400-500 µm) and large (2 mm) size where purchased from Phosphorex (Hopkinton, MA). A sampling of spheres used in study were submitted for

© 2015 Macmillan Publishers Limited. All rights reserved

DOI: 10.1038/NMAT4290

endotoxin testing by a commercial vendor (Charles River, Wilmington, MA) and the results showed that spheres contained < 0.05 EU/ml of endotoxin levels.

b. Fabrication of alginate hydrogel spheres

Alginate hydrogel spheres were made using a custom-built, electro-jetting device, consisting of a voltage generator, a vertical syringe pump, and a grounded autoclavable glass collector. The voltage was coupled to the syringe and needle containing the alginate solution while the gelling bath was grounded to complete the circuit. Spheres were generated using a 1.4% solution of a commercially available alginate (PRONOVA SLG20 (endotoxin levels or LF10/60 NovaMatrix, Sandvika, Norway) dissolved in 0.9% saline (pH ≈ 7.4, Osmotic pressure ≈ 290 mOsm), and crosslinked using a $BaCl_2$ gelling solution (20mM $BaCl_2$, 250mM D-Mannitol, 25mM HEPES, pH ≈ 7.4, Osmotic pressure ≈ 290 mOsm)[1].

Alginate hydrogel microspheres of varying sizes were generated by utilizing different needle gauges, voltages, and flow rates; 0.3 mm spheres were generated using a 30G blunt needle, a voltage of 5kV, and a 200 µl/min flow rate, 0.4 mm spheres were generated with a 25G blunt needle, a voltage of 7kV and a 200 µl/min flow rate, 0.5 mm spheres were generated with a 25G blunt needle, a voltage of 5kV and a 200 µl/min flow rate, 0.7 mm spheres were generated with a 25G blunt needle, a voltage of 4kV and a 180 µl/min flow rate, 0.9 mm spheres were generated with an 18G blunt needle, a voltage of 7kV and a 200 µl/min flow rate, 1 mm spheres were generated with an 18G blunt needle, a voltage of 6kV and a 200 µl/min flow rate, 1.5 mm spheres were generated with an 18G blunt needle, a voltage of 5kV and a 180 µl/min flow rate, and 1.9 mm spheres were generated with an 18G blunt needle with a voltage of 5 kV and a 150 µl/min flow rate. All microspheres were cross-linked in 250 mL of $BaCl_2$-gelling solution in a sterile glass container. Immediately after crosslinking, the spheres were washed with HEPES buffer (25mM HEPES, 1.2mM $MgCl_2$×6H2O, 4.7mM KCl, 132mM $NaCl_2$, pH≈7.4, ≈290 mOsm) 4 times and stored overnight at 4°C. Immediately prior to implantation into the peritoneal cavity of mice, the spheres were washed an additional 2 times with 0.9% saline. A sampling of the fabricated hydrogels was submitted for endotoxin testing by a commercial vendor (Charles River, Wilmington, MA) and the results showed that LF10/60 spheres contained 31.6 EU/mL of endotoxins while SLG20 hydrogels contained < 0.05 EU/ml of endotoxin levels.

c. Polycaprolactone (PCL) sphere synthesis

© 2015 Macmillan Publishers Limited. All rights reserved

Polycaprolactone (PCL, Mn 70,000-90,000, Sigma) microspheres were prepared by solvent evaporation with medium (0.3-0.5 mm) and large (1.5-2.0 mm) diameters. Small diameter microspheres were fabricated by dissolving PCL in dichloromethane (Fisher) at 6.5% concentration. This solution was introduced drop-wise into a 1% polyvinylalcohol (PVA, 88 mol% hydrolyzed, Polysciences Inc.) solution stirred using a stainless steel 4-blade overhead impeller at 200 rpm. After 75 min, the dispersion was added to 400 mL of ddH_2O and stirred for an additional 105 min until all of the solvent evaporated. The microspheres were then sieved, washed several times with water, flash frozen in liquid nitrogen and lyophilized overnight. Large microspheres were prepared similarly using 9% polymer concentration, 0.5% PVA solution, and a 3-blade overhead impeller stirred at 150 rpm.

d. Rat Islet Isolation, Purification, and Encapsulation

Male Sprague-Dawley rats from Jackson Laboratories (Bar Harbor, ME) weighing approximately 300 grams were used for harvesting islets. All rats were anesthetized by a 1:20 xylazine (10 mg/kg) to ketamine (150 mg/kg) injection given intraperitoneally, and the total volume of each injection was 0.4 ml – 0.5 ml depending on the weight of rat. Isolation surgeries were performed as described by Lacy and Kostianovsky[2]. Briefly, the bile duct was cannulated and the pancreas was distended by an *in vivo* injection of 0.15% Liberase (Research Grade, Roche) in RPMI 1640 media solution. Rats were sacrificed by cutting the descending aorta and the distended pancreatic organs were removed and held in 50 ml conical tubes on ice until the completion of all surgeries. All tubes were placed in a 37°C water bath for a 30 min digestion, which was stopped by adding 10-15 ml of cold M199 media with 10% heat-inactivated fetal bovine serum (HIFBS) and lightly shaking. Digested pancreases were washed twice in the same aforementioned M199 media, filtered through a 450 μm sieve, and then suspended in a Histopaque 1077 (Sigma)/M199 media gradient and centrifuged at 1,700 RCF at 4°C. Depending on the thickness of the islet layer that was formed within the gradient, this step was repeated for higher purity islets. Finally, the islets were collected from the gradient and further isolated by a series of six gravity sedimentations, in which each supernatant was discarded after four minutes of settling. Purified islets were hand-counted by aliquot under a light microscope and then washed three times in sterile 1X phosphate-buffered saline. Islets were then washed once in RPMI 1640 media with 10% HIFBS and 1% penicillin/streptomycin, and cultured in this media overnight for further use.

© 2015 Macmillan Publishers Limited. All rights reserved

DOI: 10.1038/NMAT4290

Immediately prior to encapsulation, the cultured islets were centrifuged at 1,400 rpm for 1 minute and washed with Ca-free Krebs-Henseleit (KH) Buffer (4.7mM KCl, 25mM HEPES, 1.2mM KH_2PO_4, 1.2mM $MgSO_4 \times 7H_2O$, 135mM NaCl, pH≈7.4, ≈290 mOsm). After washing, islets were centrifuged again and all supernatant was aspirated. The islet pellet was then re-suspended in a 1.4% solution of SLG20 alginate dissolved in 0.9% NaCl solution at an islet density of 1,000 islets per 0.75 ml alginate solution. Spheres were crosslinked using a $BaCl_2$ gelling solution and their sizes were controlled using similar procedures as the empty spheres (described above). Immediately after crosslinking, the encapsulated islets were washed 4 times with HEPES buffer and 2 times with RPMI Medium 1640 with 10% HIFBS and cultured overnight at 37°C for transplantation. As the islets had variable sizes (50 - 400 μm) and there was an inevitable loss of islets during the encapsulation process, the total number of encapsulated islets were recounted and converted into islet equivalents (IE, normalized to 150 μm size) based on a previously published method[3] prior to transplantation.

e. Implantation/Transplantation surgeries

All animal protocols were approved by the MIT Committee on Animal Care, and all surgical procedures and post-operative care was supervised by MIT Division of Comparative Medicine veterinary staff. Immune-competent male non-diabetic or STZ-induced diabetic C57BL/6 mice (Jackson Laboratory, Bar Harbor, ME) or male Sprague-Dawley rats (Jackson Laboratory, Bar Harbor, ME) were anesthetized with 3% isoflurane in oxygen and had their abdomens shaved and sterilized using betadine and isopropanol. Preoperatively, all mice also received a 0.05 mg/kg dose of buprenorphine subcutaneously as a pre-surgical analgesic, along with 0.3 mL of 0.9% saline subcutaneously to prevent dehydration. A 0.5 mm incision was made along the midline of the abdomen and the peritoneal lining was exposed using blunt dissection. The peritoneal wall was then grasped with forceps and a 0.5-1 mm incision was made along the linea alba. A desired volume of spheres (all materials without islets, as well as SLG20 spheres encapsulating rat islets) were then loaded into a sterile pipette and implanted into the peritoneal cavity through the incision. The incision was then closed using 5-0 taper-tipped polydioxanone (PDS II) absorbable sutures. The skin was then closed over the incision using a wound clip and tissue glue.

For non-human primate (NHP) procedures, buprenorphine (0.01-0.03 mg/kg) was administered as a pre-operative analgesic. NHPs were then sedated using an intramuscular (IM) injection of ketamine (10 mg/kg) with an addition of midazolam as dictated by DCM vet staff if

© 2015 Macmillan Publishers Limited. All rights reserved

needed for additional sedation. Animals were maintained on a circulating warm water blanket and covered with a towel during the procedure to maintain body temperature. Either 0.5 or 1.5 mm diameter SLG20 spheres were injected into the dorsal (back) regions of 4 non-human primates (cynomolgus macaques) using 18 and 12 gauge custom-manufactured (Harvard Apparatus) sterile stainless steel needles, with slip tip syringes in order to prevent shearing of our biomaterial upon injection. Needles were inserted tangentially to the backs of the NHPs, and were slid (tunneled) approximately 1-2 cm away from the initial injection point, in order to try to separate the injection from that of the site of eventual material response. Spheres (0.5 and 1.5 mm diameter) were injected into 4 total spots on the flank of 4 of our non-human primates: two spots on the left flank and two on the right, for 0.5 mm and 1.5 mm diameter sphere implants, respectively. Saline was injected and 4 mm diameter SLG20 alginate cylindrical discs were implanted by making a minimal 1 cm incision, also on the left and right sides of the back, respectively into 3 additional primates. Incisions were closed with either a single interrupted suture with 3-0 nylon or VetBond (tissue glue).

f. Blood glucose monitoring

To create insulin-dependent diabetic mice, healthy C57BL/6 mice were treated with Streptozotocin (STZ) by the vendor (Jackson Laboratory, Bar Harbor, ME) prior to shipment to MIT. The blood glucose levels of all the mice were retested prior to transplantation. Only mice whose non-fasted blood glucose levels were above 300 mg/dL for two consecutive days were considered diabetic and underwent transplantation.

Blood glucose levels were monitored three times a week following transplantation of islet-containing alginate capsules. A small drop of blood was collected from the tail vein using a lancet and tested using a commercial glucometer (Clarity One, Clarity Diagnostic Test Group, Boca Raton, FL). Mice with unfasted blood glucose levels below 200mg/dL were considered normoglycemic. Monitoring continued until all mice had returned to a hyperglycemic state at which point they were euthanized and the spheres were retrieved.

g. Retrieval of cells, tissues, and materials

At desired time points post-implantation or transplantation (with encapsulated islets), as specified in figures, mice were euthanized by CO_2 administration, followed by cervical dislocation. In certain instances, 5 ml of ice cold PBS was first injected in order perform an intraperitoneal lavage to rinse out and collect free-floating intraperitoneal immune cells. An

© 2015 Macmillan Publishers Limited. All rights reserved

DOI: 10.1038/NMAT4290

incision was then made using the forceps and scissors along the abdomen skin and peritoneal wall, and intraperitoneal lavage volumes were pipetted out into fresh 15 ml falcon tubes (each prepared with 5 ml of RPMI cell culture media). Next, a wash bottle tip was inserted into the abdominal cavity. KREBS buffer was then used to wash out all material spheres from the abdomen and into petri dishes for collection. After ensuring all the spheres were washed out or manually retrieved (if fibrosed directly to intraperitoneal tissues), they were transferred into 50 mL conical tubes for downstream processing and imaging. After intraperitoneal lavage and sphere retrieval, remaining fibrosed intraperitoneal tissues were also excised for downstream FACS and expression analyses.

For non-human primate subcutaneous retrievals, similar to when material was implanted, NHPs were once again given buprenorphine (0.01-0.03 mg/kg) as a pre-operative analgesic, and sedated using an IM injection of ketamine (10 mg/kg), with midazolam as dictated by DCM vet staff if needed for additional sedation. Animals were once again maintained on a circulating warm water blanket and covered with a towel during the procedure to maintain body temperature. 8 mm diameter biopsy punches were then used to sample the entire skin and subcutaneous space at 2 and later at 4 weeks post-implantation. Following biopsy punches, the retrieval site was closed with 3-0 nylon in a simple-interrupted pattern and VetBond (tissue glue).

h. Imaging of the retrieved material spheres

For phase contrast imaging retrieved materials were gently washed using Krebs buffer and transferred into 35 mm petri dishes for phase contrast microscopy using an Evos Xl microscope (Advanced Microscopy Group).

For bright-field imaging of retrieved materials, samples were gently washed using Krebs buffer and transferred into 35 mm petri dishes for bright-field imaging using a Leica Stereoscopic microscope.

i. Newport Green and Live/Dead Islet Staining

LIVE/DEAD® Viability/Cytotoxicity Kit (Life technologies, Carlsbad CA; CA# L-3224) was used according to the manufacturer's instructions to assess the viability of islets post-encapsulation. Newport Green™ DCF Diacetate (Life technologies, Carlsbad CA; CA# N-7991), cell permeant dye combined with DAPI was used to stain encapsulated islet cells post-retrieval.

j. Confocal Immunofluorescence

© 2015 Macmillan Publishers Limited. All rights reserved

Immunofluorescence imaging was used to determine immune populations attached to spheres. Materials were retrieved from mice and fixed overnight using 4% paraformaldehyde at 4°C. Samples where then washed twice with KREBS buffer, permeabilized for 30 min using a 0.1% Triton X100 solution, and subsequently blocked for 1 hour using a 1% bovine serum albumin (BSA) solution. Next, the spheres were incubated for 1 hour in an immunostaining cocktail solution consisting of DAPI (500 nM), specific marker probes (1:200 dilution) in BSA. After staining, spheres were washed three times with a 0.1% Tween 20 solution and maintained in a 50% glycerol solution. Spheres were then transferred to glass bottom dishes and imaged using an LSM 700 point scanning confocal microscope (Carl Zeiss Microscopy, Jena Germany) equipped with 5 and 10X objectives. Obtained images where adjusted linearly for presentation using Photoshop (Adobe Inc. Seattle, WA).

k. Histological processing for H&E and Masson's Trichrome staining

Retrieved materials where fixed overnight using 4% paraformaldehyde at 4°C. After fixation, alginate sphere or retrieved tissue samples were washed using 70% alcohol. The materials where then mixed with 4 degrees calcium-cooled Histogel (VWR, CA # 60872-486). After the molds hardened, the blocks were processed for paraffin embedding, sectioning and staining according to standard histological methods.

l. Western Blotting

Protein was extracted directly from materials for western blot analysis. For protein analyses, retrieved materials were prepared by immersing materials in Pierce RIPA buffer (Cat. #89901, Thermo Scientific) with protease inhibitors (Halt Protease inhibitor single-use cocktail, Cat. #78430, Thermo Scientific) on ice, and then lysed by sonication (for 30 seconds on, 30 seconds off, twice at 70% amplitude). Samples were then subjected to constant agitation for 2 hours at 4°C. Lysates were then centrifuged for 20 min at 12,000 rpm at 4°C, and protein-containing supernatants were collected in fresh tubes kept on ice. In samples from fat tissue, an excess of fat (a top layer on the supernatant) was first removed before supernatant transfer. 20 μg protein (quantified by BCA assay, Pierce BCA protein assay kit, Cat. #23225, Thermo Scientific) for each lane was boiled at 95°C for 5 min and electrophoresed on SDS-polyacrylamide gels (Any kD 15-well comb mini-gel, Biorad, Cat. #456-9036) and then blotted onto nitrocellulose membranes (Biorad, Cat. #162-0213). Blots were probed with anti-αSmooth Muscle actin

© 2015 Macmillan Publishers Limited. All rights reserved

DOI: 10.1038/NMAT4290

antibody (1:400 dilution, Rabbit polyclonal to alpha smooth muscle actin; Cat. #ab5694, AbCam), anti-PDX1 antibody (1:1000 dilution, Rabbit polyclonal to pancreatic & duodenal homeobox 1; Cat. #06-1379, EMD Millipore), and anti-β-actin antibody (1:4000 dilution, monoclonal anti-β-actin antibody produced in mouse; Cat. #A1978, Sigma Aldrich) as a loading control followed by donkey anti-rabbit (1:15,000 dilution, Cat. #926-32213, Li-Cor) and goat anti-mouse (1:15,000 dilution, Cat. #926-68070, Li-Cor) fluorophore-conjugated secondary antibodies. Antibody-antigen complexes were visualized using Odyssey detection (Li-Cor, Serial No. ODY-2329) at 700 and 800 nm wavelengths.

m. qPCR analysis

Total RNA was isolated from tissue (peripheral tissue alone, spheres alone and/or with adhered cells and fibrotic overgrowth, if present, and ip lavage alone), liquid nitrogen snap-frozen immediately following excision, using TRIzol (Invitrogen; Carlsbad, CA) according to the manufacturer's instructions. In addition, to help ensure complete tissue disruption, we also employed strong mechanical disruption with a Polytron homogenizer. Thus, gene expression signatures shown throughout are proportional and representative of the entire cell population present on and/or around retrieved materials. Before reverse transcription using the High Capacity cDNA Reverse Transcription kit (Cat. #4368814; Applied Biosystems, Foster City, CA), all samples were first normalized for comparison by loading the same input 1 μg total RNA in a volume of 20 μl for each sample. cDNA (4.8 μl; 1:20 dilution) in a total volume of 16 μl (including SYBR Green and PCR primers) was amplified by qPCR with the following primers. Primers (Table S2) were designed using Primer Express software (Applied Biosystems, Carlsbad, CA, USA) and evaluated using LaserGene software (DNAStar, Madison, WI, USA) to ensure either mouse or rat (host)-specificity. Samples were incubated at 95°C for 10 min followed by 40 cycles of 95°C for 15 sec and 60°C for 1 min in an ABI PRISM 7900HT Sequence Detection System (Applied Biosystems). Results were analyzed using the comparative C_T (DDC_T) method as described by the manufacturer. Results were analyzed using the comparative C_T ($\Delta\Delta C_T$) method and are presented as relative RNA levels compared to the RNA expression in either mock-implanted control cell samples (peripheral intraperitoneal fat tissue, or free floating intraperitoneal lavage cells) after normalization to the β-actin RNA content of each sample. For material spheres alone, we compared everything relative to either 0.3 or 0.5 mm alginate SLG20 spheres. In addition, to further ensure proper normalization and sample handling across multiple

© 2015 Macmillan Publishers Limited. All rights reserved

retrieval time points, RNA for all samples for each harvest condition (ie., ip lavage, spheres with or without adhered cells and fibrosis, and peripheral tissues with infiltration, as described), were quantified, reverse transcribed, and analyzed by qPCR in parallel. Mouse-specific (host) or rat (islet)-specific forward and reverse primer sets were utilized for this study (Supplemental Table S2).

n. ELISpot multiplexed cytokine analysis

Cytokine array analysis was performed using the Proteome Profiler Mouse Cytokine Array Panel A kit (Cat. #ARY006, R&D Systems). For this analysis, proteins were extracted directly from materials, as described above in the western blotting section. For each membrane, 200 µl of protein solution was mixed with 100 µl of sample buffer (array buffer 4) and 1.2 ml of block buffer (array buffer 6), then added with 15 µl of reconstituted Mouse Cytokine Array Panel A Detection Antibody Cocktail and incubated at room temperature for 1 hour. The array membrane was incubated with block buffer (array buffer 6) for 2 hours on a rocking platform shaker. The block buffer was then aspirated, and the prepared sample/antibody mixture was added onto the membrane and incubated overnight at 4°C on a rocking platform shaker. The membrane was washed three times with 20 ml of 1X wash buffer for 10 minutes on a rocking platform shaker, rinsed once with deionized water, then probed with Fluorophore-conjugated streptavidin (1:5,000 dilution, Cat. #926-32230, Li-Cor) at room temperature for 30 minutes on a rocking platform shaker, and then washed with wash buffer three more times and with deionized water once again, as described above. Antibody-antigen complexes were visualized using Odyssey Detection (Li-Cor, Serial No. ODY-2329) at a 800 nm wavelength. The densities of the spots were analyzed using Image J software.

o. Real-time fluorescence imaging of islet intracellular calcium

Real-time fluorescence imaging of islet intracellular calcium $[Ca^{2+}]_i$ was performed in a microfluidic device modified for encapsulated islets[4]. In brief, fifty Sprague Dawley rat islets naked or encapsulated in alginate capsules (0.5 mm and 1.5 mm diameter) were incubated with 5 µM Fura-2/AM (a calcium indicator, Molecular Probes, CA, USA) at 37°C in Krebs-Ringer buffer (KRB) supplemented with 2 mM glucose (KRB2) and 0.5% BSA for 35 min. The islets were then loaded into the microfluidic device mounted on an inverted epifluorescence microscope (Leica DMI 400B, IL, USA). Excess dye was washed out with KRB2 for 35 min at 500 µL/min. Dual-wavelength Fura-2/AM dye were excited ratiometrically at 340 and 380 nm,

© 2015 Macmillan Publishers Limited. All rights reserved

DOI: 10.1038/NMAT4290

and changes in the $[Ca^{2+}]_i$ levels are expressed as F340/F380 (% increase from basal 2 mM glucose). Excitation wavelengths were controlled by excitation filters (Chroma Technology, VT, USA) mounted in a Lambda DG-4 wavelength switcher. Emission of Fura-2/AM was filtered using a Fura2/FITC polychroic beamsplitter and a double band emission filter (Chroma Technology. Part number: 73.100bs). SimplePCI software (Hamamatsu Corp, IL, USA) was used for imaging acquisition and analysis. These images were collected with a high-speed, high-resolution charge coupled camera (CCD, Retiga-SRV, Fast 1394, QImaging).

Individual islet intracellular calcium responses were assessed with the following perifusion protocol: 1) KRB2 (0-5 min); 2) 20 mM glucose (5-25 min); 3) KRB2 (25-45 min); 4) 30 mM KCl (45-60 min); 5) KRB2 (60-70 min). The area under the curve for each time period was calculated for each individual islet in order to statistically compare groups using one-way ANOVA ($p < 0.05$ as significant). Three separate batches of rodent isolations were used for assessments where each condition was tested from the same batch of islets (naked islets n = 59; 0.5 mm n = 49; 1.5 mm n = 43).

p. Insulin secretion kinetics

Islet insulin responses were assessed by loading 50 rat islets naked or encapsulated at 0.5 mm and 1.5 mm alginate capsules into the same microfluidic device used for calcium measurements. Perifusate samples were collected every minute (500 μL/min) by an automated fraction collector (Gilson, model 203B, WI, USA). Insulin concentrations were quantified every other minute using a rodent chemiluminescent insulin ELISA (Alpco, NH, USA). The following perifusion protocol was used: 1) KRB2 (0-20 min); 2) 20 mM glucose or 30 mM KCl (20-55 min); 3) KRB2 (55-100 min). The area under the curve for each insulin curve (n=3 for naked, 0.5 mm, and 1.5 mm) was calculated in order to statistically compare groups using one-way ANOVA ($p < 0.05$ as significant).

q. FACS analysis

Single-cell suspensions of freshly excised tissues were prepared using a gentleMACS Dissociator (Miltenyi Biotec, Auburn, CA) according to the manufacturer's protocol. Single-cell suspensions were prepared in a passive PEB dissociation buffer (1X PBS, pH 7.2, 0.5% BSA, and 2 mM EDTA) and suspensions were passed through 70 μm filters (Cat. #22363548, Fisher Scientific, Pittsburgh, PA). This process removed the majority of cells adhered to the surface

© 2015 Macmillan Publishers Limited. All rights reserved

(>90%) (See **Supplemental Figure 17**). All tissue and material sample-derived, single-cell populations were then subjected to red blood cell lysis with 5 ml of 1X RBC lysis buffer (Cat. #00-4333, eBioscience, San Diego, CA, USA) for 5 min at 4°C. The reaction was terminated by the addition of 20 ml of sterile 1X PBS. The cells remaining were centrifuged at 300-400g at 4°C and resuspended in a minimal volume (~50 µl) of eBioscience Staining Buffer (cat. #00-4222) for antibody incubation. All samples were then co-stained in the dark for 25 min at 4°C with two of the fluorescently tagged monoclonal antibodies specific for the cell markers CD68 (1 µl (0.5 µg) per sample; CD68-Alexa647, Clone FA-11, Cat. #11-5931, BioLegend), Ly-6G (Gr-1) (1 µl (0.5 µg) per sample; Ly-6G-Alexa-647, Clone RB6-8C5, Cat. #108418, BioLegend), CD11b (1 µl (0.2 µg) per sample; or CD11b-Alexa-488, Clone M1/70, Cat. #101217, BioLegend). Two ml of eBioscience Flow Cytometry Staining Buffer (cat. #00-4222, eBioscience) was then added, and the samples were centrifuged at 400-500g for 5 min at 4°C. Supernatants were removed by aspiration, and this wash step was repeated two more times with staining buffer. Following the third wash, each sample was resuspended in 500 µl of Flow Cytometry Staining Buffer and run through a 40 µm filter (Cat. #22363547, Fisher Scientific) for eventual FACS analysis using a BD FACSCalibur (cat. #342975), BD Biosciences, San Jose, CA, USA). For proper background and laser intensity settings, unstained, single antibody, and IgG (labled with either Alexa-488 or Alexa-647, BioLegend) controls were also run.

r. Intravital Imaging and MAFIA depletion

For intravital imaging, SLG20 hydrogels of 0.5 mm and 1.5 mm sizes were loaded with Qdot 605 (Life technologies, Grand Island, NY) and surgically implanted into C57BL/6-Tg(Csf1r-EGFP-NGFR/FKBP1A/TNFRSF6)2Bck/J mice as described above. After 1, 4, or 7 days post implantation, the mice were placed under isoflurane anesthesia and a small incision was made at the site of the original surgery to expose beads. The mice were placed on an inverted microscope and imaged using a 25x, N.A. 1.05 objective on an Olympus FVB-1000 MP multiphoton microscope at an excitation wavelength of 860 nm. Z-stacks of 200 µm (10 µm steps) were acquired at 2-minute intervals for time series of 20 - 45 minutes depending on the image. The mice were kept under constant isoflurane anesthesia and monitored throughout the imaging session. Obtained images were analyzed using Velocity 3D Image Analysis Software (Perkin Elmer, Waltham, MA).

© 2015 Macmillan Publishers Limited. All rights reserved

DOI: 10.1038/NMAT4290

In addition, to investigate fibrosis or the lack thereof in control (non-depleted) or induced macrophage-depleted MAFIA mice, 0.5 mm SLG20 spheres were transplanted as described above. In the case of targeted macrophage depletion, an additional group of n = 5 mice were injected intravenously (tail vein) with B/B homodimerizer (Clontech). We achieved significant macrophage depletion (~80-90%, mean group decrease = 84.36%, **Supplemental Figure S13c**) following our administering of an intravenous injection of 10 mg/kg of the homodimerizer AP20187 in these mice. Repeat depletion in the MAFIA model three days prior and then once every 3 days, starting 3 days following alginate sphere implantation up until retrieval, was able to knock down macrophage numbers far below peritoneal levels observed in the IP space of transplanted, non-depleted control MAFIA mice (~65.26% vs ~10.2%; **Supplemental Figure S13c)**.

s. NanoString analysis

RNAs for mock-implanted/mock-treated (MT) controls, or for 0.5 or 1.5 mm alginate sphere-bearing mice (n = 4/group) were isolated from tissue samples taken at various time points after implantation, as described. Respective RNAs were quantified, diluted to the appropriate concentration (100 ng/μl), and then 500 ng of each sample was processed according to NanoString manufacturer protocols for expression analysis via our customized multiplexed gene mouse macrophage subtyping panel. RNA levels (absolute copy numbers) were obtained following nCounter (NanoString Technologies Inc., Seattle, WA) quantification, and group samples were analyzed using nSolver analysis software (NanoString Technologies Inc., Seattle, WA).

t. Statistical analysis

Data are expressed as mean ± SEM, and N = 5 mice per time point and per treatment group. For Rat studies N = 3 per treatment. These sample sizes where chosen based on previous literature. All animals were included in analyses except in instances of unforeseen sickness or morbidity. Animal cohorts where randomly selected. Investigators where not blind to performed experiments. For qPCR or FACS, data were analyzed for statistical significance either by unpaired, two-tailed t-test, or one-way ANOVA with Bonferroni multiple comparison correction, unless indicated otherwise, as implemented in GraphPad Prism 5; *: $p < 0.05$, **: $p < 0.001$, and ***: $p < 0.0001$. High throughput NanoString based gene expression analysis data was divided

© 2015 Macmillan Publishers Limited. All rights reserved

into sets based on macrophage subtype and compartment. Data was normalized using the geometric means of the NanoString positive controls and background levels were established using the means of the negative controls. Housekeeping genes Tubb5, Hprt1, Bact, and Cltc were used to normalize between samples. Data was then log-transformed. For each subtype, time, and compartment group, a two-way ANOVA for the effect of size blocking on genes was performed. P-values were computed from pairwise comparisons performed using Tukey's Honest Significant Difference test and the Bonferroni correction was used to control the overall error rate.

2. Supplemental Discussion

Diffusion of insulin and glucose as a function of capsule geometry

In beta-cells, glucose-induced insulin secretion is a complex process involving glucose metabolism, mitochondrial energy production, potassium-dependent ATP channels (K_{ATP} channels), voltage-dependent calcium channels (VDCCs), calcium influx, and insulin secretion, which has a biphasic and oscillatory kinetic pattern[5]. In this study, we applied a microfluidic perifusion device to dynamically measure intracellular calcium influx (a downstream and immediately proximal trigger for the fusion of insulin granules to the plasma membrane and exocytosis) and insulin concentrations in perifusate samples in order to characterize the impact of encapsulation and capsule size on insulin secretion coupling factors and insulin secretion. As shown in **Supplemental Figure 11A**, glucose-induced intracellular calcium signals were similar among the three groups with typical phase responses in all three groups. No significant differences were observed from the start time of calcium influx up to the maximal calcium peak in response to both 20 mM glucose and 30 mM KCl (potassium chloride) challenge. Additionally, the areas under the curve (AUCs) of calcium concentrations under both stimulators were not significantly different (**Supplemental Figure 11B**). However, the time to reach the maximal calcium level for the 1.5 mm capsules was statistically delayed in response to glucose compared to the naked islets and 0.5 mm capsules ($p = 0.03$), but not statistically delayed in response to KCl stimulation.

Our results suggest that small molecules, such as glucose (180.2 daltons) and KCl (74.6 daltons), diffuse very rapidly into the alginate capsules and efficiently induce calcium influx at a

© 2015 Macmillan Publishers Limited. All rights reserved

DOI: 10.1038/NMAT4290

similar rate as naked islets. This suggests that the encapsulation process and alginate material do not acutely impede glucose metabolism or insulin stimulator-secretion coupling factors such as mitochondrial energy production and ion channels that are important for *in vitro* and *in vivo* function. Furthermore, diffusion efficiency in the capsule may depend on molecular weight of the analyte since there was a delayed time to reach a maximal calcium level in the 1.5 mm capsules in response to glucose (180.2 daltons), but not to KCl (74.6 daltons).

Next, we investigated the insulin secretion kinetics of the naked and encapsulated islets. As shown in **Supplemental Figure 12A**, naked islets show typical biphasic insulin secretion patterns in response to glucose, while both encapsulated islet groups show loss of the biphasic pattern showing that insulin secretion gradually increases over the period of glucose stimulation without a defined phase I secretion. No significant differences were observed from the start time of insulin secretion up to the maximal peak insulin secretion in response to both 20 mM glucose and 30 mM KCl challenges. However, the times to reach maximal insulin secretion from 20 mM glucose and 30 mM KCl were significantly delayed for 0.5 mm and 1.5 mm encapsulated islets compared to naked islets (p = 0.0002 (20mM glucose), 0.04 (30 mM KCl)). Further analysis of insulin secretory kinetic curves showed that the total insulin secreted by naked islets in the first ten minutes of stimulation was significantly higher than for both 0.5 mm- and 1.5 mm-encapsulated islets in responses to both glucose and KCl (p = 0.02 and 0.04, respectively), but not significantly different for later time segments during stimulation. This data further suggests that the larger molecular weight of the insulin (5,808 Da) is the determining factor resulting in longer diffusion time through the alginate gel into the perifusate chamber for both encapsulated groups compared to naked islets.

Total insulin secreted by all groups during stimulation (20-55 min) and during the wash out period after stimulation (55-100 min) was also found not to be significantly different in response to both stimulators (**Supplemental Figure 12C and D**). This suggests that overall bulk insulin secretion is unaffected by encapsulation or capsule size. More importantly, encapsulated islets returned to basal insulin secretory levels similar to naked islets, which is a critical factor when considering future clinical application as prolonged insulin secretion after stimulation could cause dangerous hypoglycemia.

Together with normal glucose-induced calcium influx, our results indicate that the altered insulin secretion profiles of the encapsulated islets seem to be largely affected by the presence of an alginate gel due to increasing diffusion time of larger MW insulin from the capsule to the perifusate. This may explain the observed loss of phase I insulin secretion of encapsulated islets

© 2015 Macmillan Publishers Limited. All rights reserved

in response to glucose. However, there is no significant difference in insulin secretory kinetics between 0.5 mm- and 1.5 mm-encapsulated islets, suggesting capsule size has little effect on insulin secretion.

In summary, islet stimulation kinetics by small molecular weight secretagogues is unaffected by encapsulation or capsule size; however, initial insulin secretory kinetics are delayed similarly for encapsulated islets at both capsule sizes. Nonetheless, overall bulk insulin kinetics for both capsule sizes are well-conserved and similar to naked islets.

© 2015 Macmillan Publishers Limited. All rights reserved

DOI: 10.1038/NMAT4290

3. Supplementary Tables:

Table S1. P-values indicating level of significance for comparisons between mock surgeries and implanted SLG20 spheres innate immune responses over time classified by macrophage markers, size, and days after implantation. Nanostring data was log-transformed and a linear model consisting of time, size, gene, compartment, and macrophage type was constructed. Pairwise comparisons between the mock and implanted groups were performed using Tukey's range test. Significance level $\alpha = 0.05$. N=4 mice per treatment. For details of analysis see supplemental methods description.

Compartment	Type	Day 1			Day 4			Day 7	
		0.5 mm	1.5 mm		0.5 mm	1.5 mm		0.5 mm	1.5 mm
Intraperitoneal Space	Classic	0.5832	1.0000		0.0168	1.0000		0.0017	0.8812
	Regulatory	1.0000	1.0000		1.0000	1.0000		1.0000	1.0000
	Wound	0.0001	0.0097		<0.0001	0.0041		<0.0001	0.1455
Fat	Classic	1.0000	1.0000		0.2175	0.2302		0.0326	0.5249
	Regulatory	1.0000	1.0000		0.8362	0.6927		1.0000	1.0000
	Wound	0.9603	1.0000		<0.0001	0.0075		0.0001	1.0000
Spheres	Classic	0.0001	1.0000		<0.0001	<0.0001		<0.0001	<0.0001
	Regulatory	1.0000	1.0000		0.0089	0.5295		<0.0001	1.0000
	Wound	<0.0001	<0.0001		<0.0001	<0.0001		<0.0001	<0.0001

© 2015 Macmillan Publishers Limited. All rights reserved

Table S2. Mouse (m) or rat (r)-specific (host) forward and reverse primer sets used for qPCR analysis of RNA levels. Gene names are also shown in parentheses.

Gene	Primers (5' to 3'): Sense & Antisense
Mouse Collagen 1a1 (m*Col1a1*)	Forward: 5'-CATGTTCAGCTTTGTGGACCT-3'
	Reverse: 5'-GCAGCTGACTTCAGGGATGT-3'
Mouse Collagen 1a2 (m*Col1a2*)	Forward: 5'-GCAGGTTCACCTACTCTGTCCT-3'
	Reverse: 5'-CTTGCCCCATTCATTTGTCT-3'
Mouse Alpha Smooth Muscle actin (m*Acta2*)	Forward: 5'-CGCTTCCGCTGCCCAGAGACT-3'
	Reverse: 5'-TATAGGTGGTTTCGTGGATGCCCGCT-3'
Mouse Myeloid cell marker CD11b (m*Itgam*)	Forward: 5'-CCAAGAGAATGCAAAAGGCTTT-3'
	Reverse: 5'-GGGGGGCTGCAACAACCACA-3'
Mouse Macrophage marker CD68 (m*Cd68*)	Forward: 5'-GCCCGAGTACAGTCTACCTGG-3'
	Reverse: 5'-AGAGATGAATTCTGCGCCAT-3'
Mouse neutrophil marker Gr1 (m*Ly6g*)	Forward: 5'-TGCCCCTTCTCTGATGGATT-3'
	Reverse: 5'-TGCTCTTGACTTTGCTTCTGTGA-3'
Mouse β-actin (m*ActB*)	Forward: 5'-GCTTCTTTGCAGCTCCTTCGTT-3'
	Reverse: 5'-CGGAGCCGTTGTCGACGACC-3'
Rat Collagen 1a1 (r*Col1a1*)	Forward: 5'-CATGTTCAGCTTTGTGGACCT-3'
	Reverse: 5'-GCAGCTGACTTCAGGGATGT-3'
Rat Collagen 1a2 (r*Col1a2*)	Forward: 5'-CCTGGCTCTCGAGGTGAAC-3'
	Reverse: 5'-CAATGCCCAGAGGACCAG-3'
Rat Alpha Smooth Muscle actin (r*Acta2*)	Forward: 5'-TGCCATGTATGTGGCTATTCA-3'
	Reverse: 5'-ACCAGTTGTACGTCCAGAAGC-3'
Rat Pdx1 (r*Pdx1*)	Forward: 5'-CTCTCGTGCCATGTGAACC-3'
	Reverse: 5'-TTCTCTAAATTGGTCCCAGGAA-3'
Rat β-actin (r*ActB*)	Forward: 5'-ACCTTCTTGCAGCTCCTCCGTC-3'
	Reverse: 5'-CGGAGCCGTTGTCGACGACG-3'

© 2015 Macmillan Publishers Limited. All rights reserved

DOI: 10.1038/NMAT4290

4. Supplementary Figures:

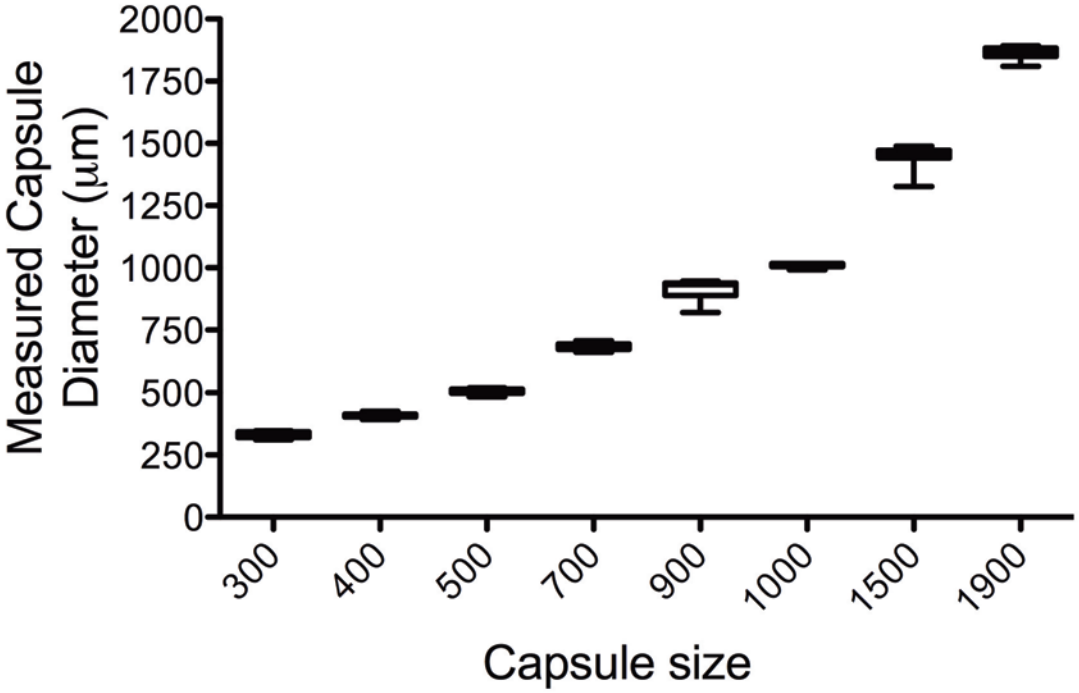

Supplementary Figure S1. Alginate hydrogel microspheres of 8 sizes where prepared with narrow size distributions. Box and whisker plot of measured sphere sizes determined through measurement of 10 randomly selected spheres from each size group. Two different batches of preparations were separately analyzed.

© 2015 Macmillan Publishers Limited. All rights reserved

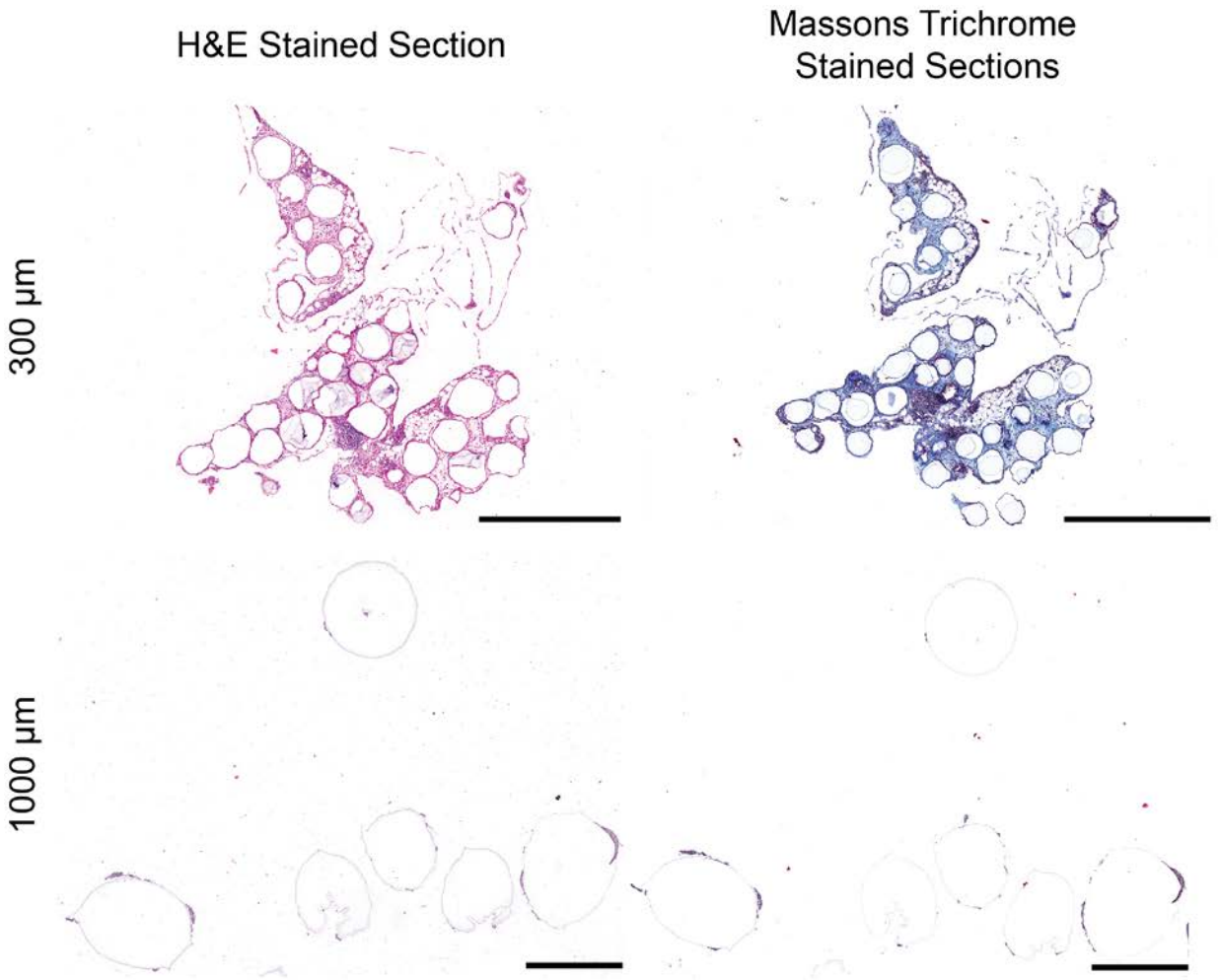

Supplemental Figure S2. H&E (*left*) and Masson's trichrome (*right*) staining of SLG20 alginate hydrogel microspheres. Small (0.3 mm diameter) (*top*) and large (1 mm diameter) (*bottom*) sizes retrieved after 14-day implantation in the intraperitoneal space of C57BL/6 mice; Scale bar = 1 mm. N=5 mice per treatment. Imaging experiments were repeated 3 times.

© 2015 Macmillan Publishers Limited. All rights reserved

DOI: 10.1038/NMAT4290

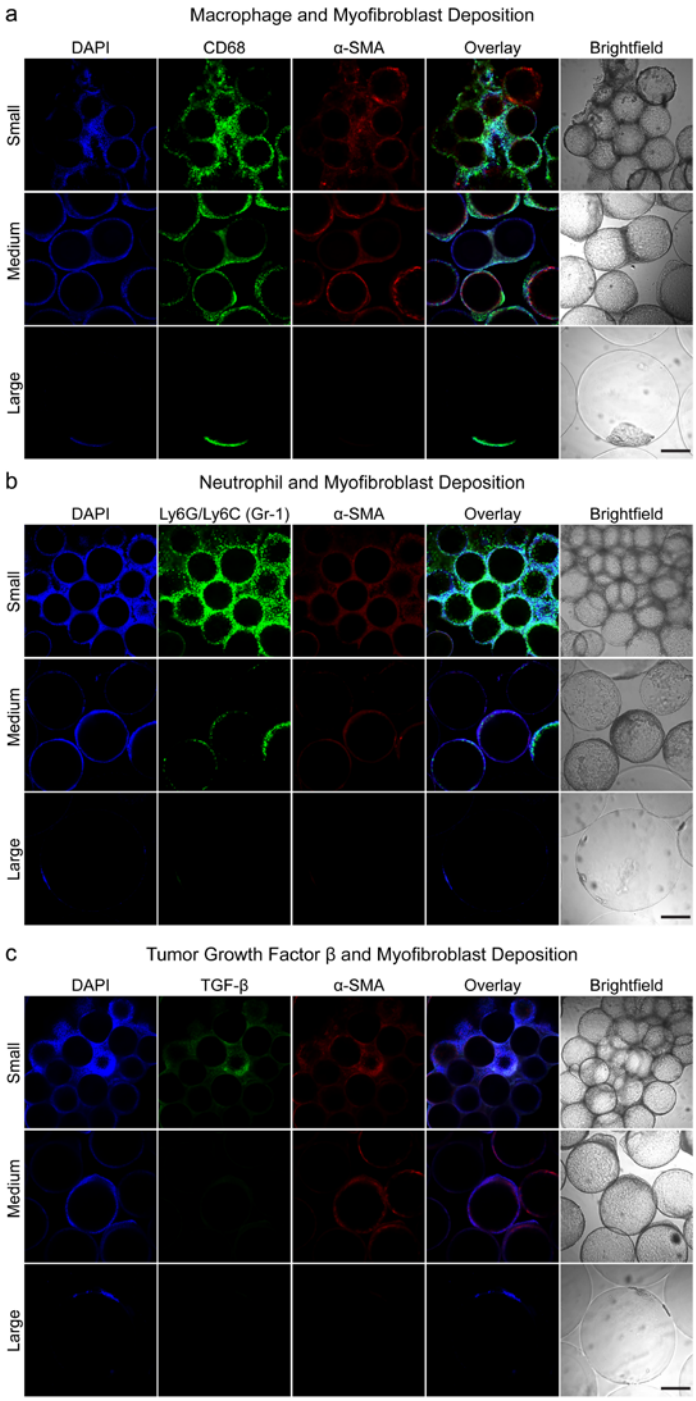

Supplemental Figure S3. Immunofluorescence confocal images of SLG20 alginate hydrogel microspheres of small (0.3 mm), medium (0.5 mm), and large (1 mm) sizes retrieved after a 14-day implantation into the intraperitoneal space of C57BL/6 mice. In all cases, staining for cell nuclei (DAPI, blue) and fibrosis-associated activated myofibroblasts (α-SMA, red) was performed, rotating (green) stains for macrophages (CD68) **(a)**, neutrophils (Ly6G/Ly6C Gr-1) **(b)**, or Tumor Growth Factor β (TGFβ) (**c**), as noted. Scale bar = 300 μm. N=5 mice per treatment. Imaging experiments were repeated 3 times.

© 2015 Macmillan Publishers Limited. All rights reserved

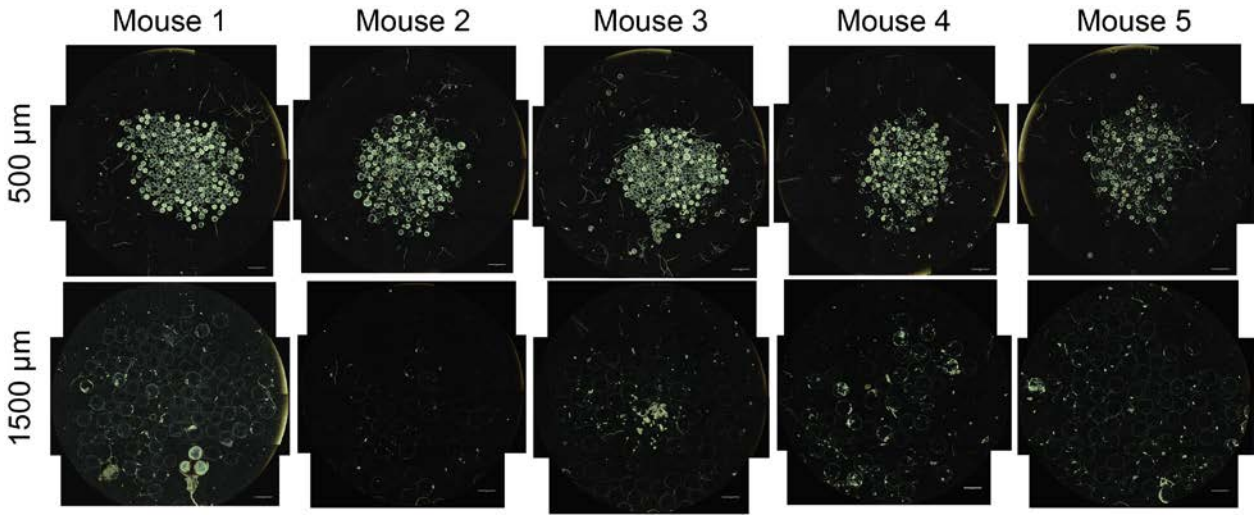

Supplemental Figure S4. Phase contrast images from retrieved Ba-crosslinked SLG20 spheres of 0.5 mm, and 1.5 mm diameter spheres normalized by equivalent total surface area implanted into the intraperitoneal space of C57BL/6 mice. Note: to generate an equivalent surface area, 9 times fewer individual 1.5 mm spheres are needed than those for the 0.5 mm size; based on the difference in volume between the 0.5 mm and 1.5 mm spheres (27-fold greater for the 1.5 mm size), this numerical difference translated into a net 3-fold greater total implant volume (300 µl vs 100 µl) for the 1.5 mm spheres over that for the 0.5 spheres. Images obtained from all spheres retrieved from individual mice (n = 5/group). Medium (0.5 mm) spheres were heavily clumped and fibrosed, and large (1.5 mm) spheres were clear/translucent, due to a lack of visible fibrotic deposition. The same material volume of hydrogel spheres was implanted into each mouse (n = 5/group) in all cases. Scale bar = 2 mm. Experiments were repeated twice.

© 2015 Macmillan Publishers Limited. All rights reserved

DOI: 10.1038/NMAT4290

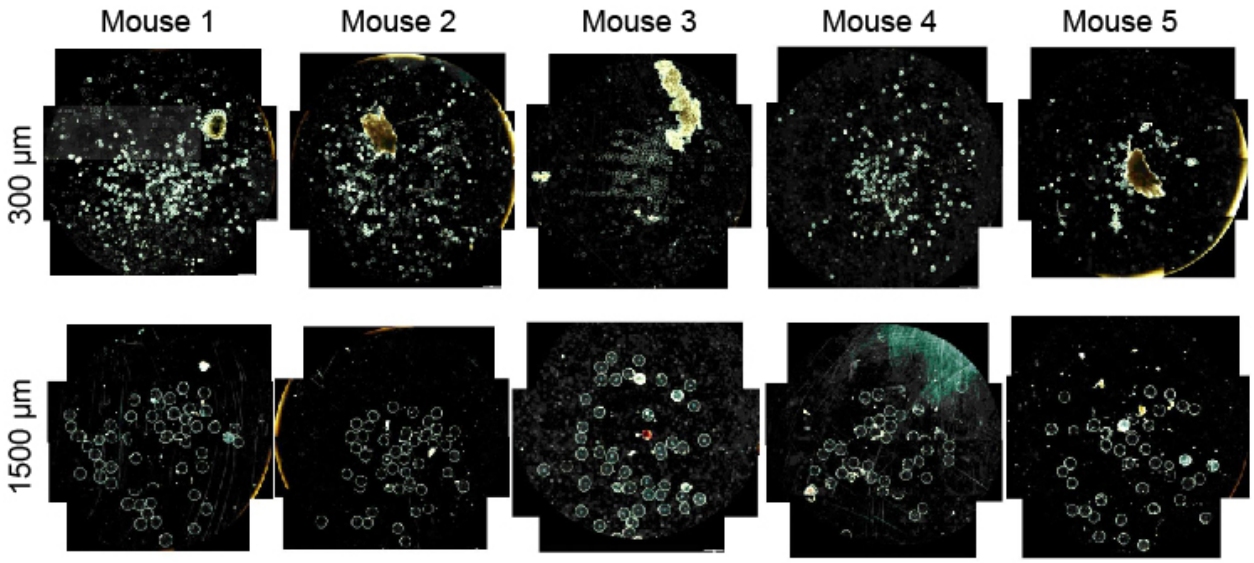

Supplemental Figure S5. Phase contrast images from retrieved Ba-crosslinked SLG20 microspheres of small (0.3 mm), and large (1.5 mm) sizes 6 months post-intraperitoneal implant into C57BL/6 mice. Small (0.3 mm) spheres were heavily clumped and fibrosed, and large (1.5 mm) spheres were clear/translucent, due to a lack of visible fibrotic deposition. The same material volume of hydrogel spheres was implanted into each mouse (n = 5/group) in all cases. Scale bar = 2 mm. Experiments were repeated twice.

© 2015 Macmillan Publishers Limited. All rights reserved

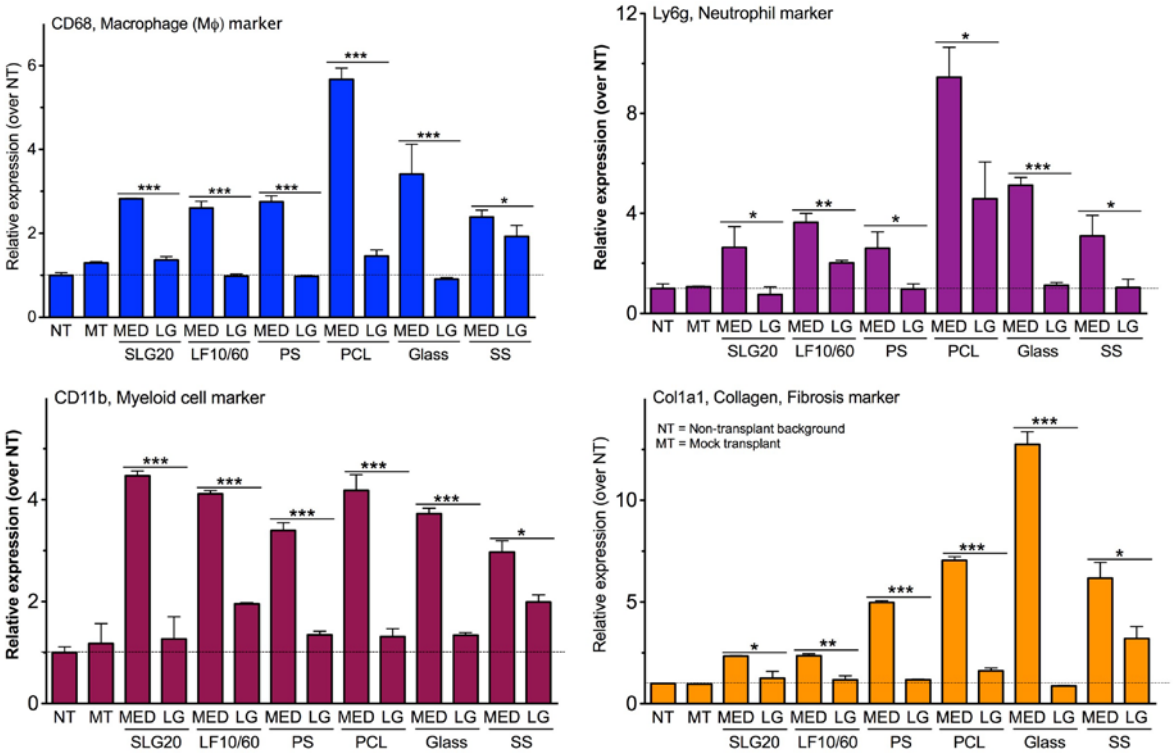

Supplemental Figure S6. qPCR panels showing that the effect of increased size in reducing foreign body responses expands across a spectrum of materials including hydrogels, plastics, metals, and ceramics. Medium (MED, 0.4-0.6 mm) or large sized (LG, 1.5-2.5 mm) spheres were implanted into the intraperitoneal space of C57BL/6 mice. All materials were then retrieved 14 days post-implant, and levels of different innate immune and fibrosis markers were assayed by gene expression. CD68, macrophage marker; Ly6g/Gr1, neutrophil marker; CD11b, myeloid cell marker; and Col1a1, collagen marker. Materials: SLG20 (chemically purified alginate), LF10/60 (non-purified, endotoxin-containing alginate), polymers polystyrene (PS) and PCL (polycaprolactone), silica-based ceramic glass, and stainless steel (SS). Note on plots NT= No treatment, and MT= Mock Treatment (i.e. PBS injection alone). Error bars, mean ± SEM. N=5 mice per treatment. qPCR statistical analysis: one-way ANOVA with Bonferroni multiple comparison correction *: $p < 0.05$, **: $p < 0.001$, and ***: $p < 0.0001$, comparing MED vs. LG. Experiments were repeated twice.

© 2015 Macmillan Publishers Limited. All rights reserved

DOI: 10.1038/NMAT4290

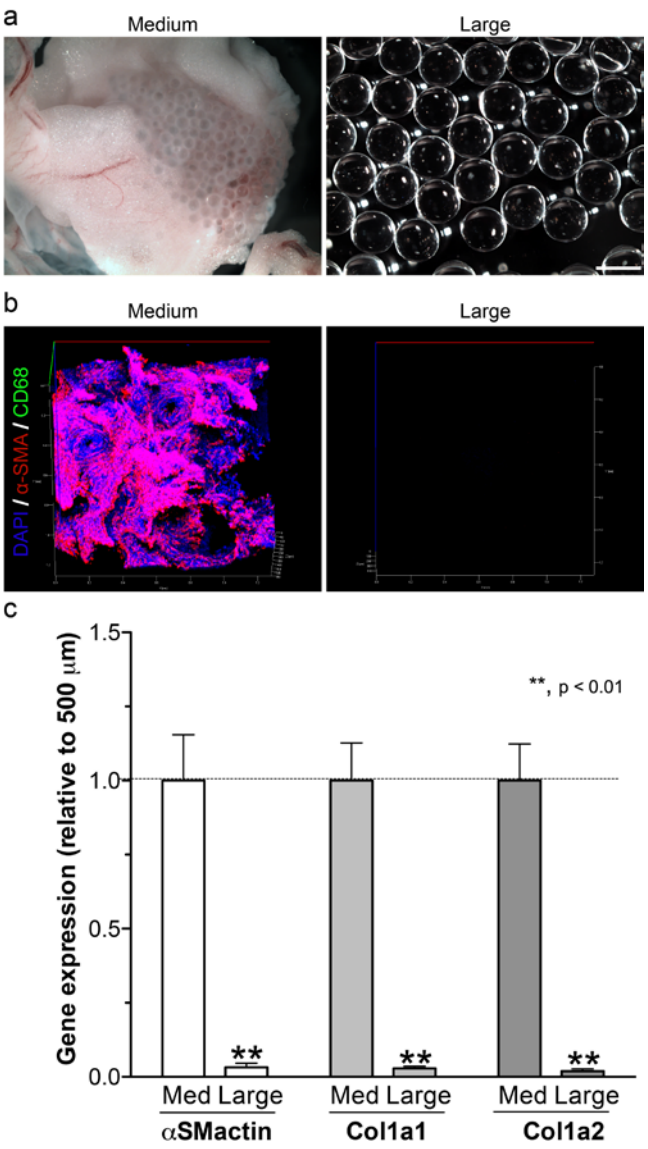

Supplemental Figure S7. Fibrosis deposition onto medium (0.5 mm) and large sized (2mm) glass microspheres implanted into the peritoneal cavity of Sprague-Dawley rats and retrieved after two 2 weeks. Representative brightfield images of retrieved spheres showing extensive fibrotic/cellular overgrowth; scale bars = 2 mm (**a**). Representative immunofluorescence Z-stacked confocal image of microspheres Stains used: for cell nuclei (DAPI, blue), macrophages (CD68, green) and fibrosis-associated activated myofibroblasts (α-SMA, red) (**b**). q-PCR based expression analysis of fibrotic markers α-SMA, Collagen 1a1 (Col1a1), and Collagen 1a2 (Col1a2) directly on medium and large sized glass microspheres plotted normalized to relative expression levels onto medium sized spheres (**c**). Error bars, mean ± SEM. N=3 rats per treatment. qPCR statistical analysis: one-way ANOVA with Bonferroni multiple comparison correction **: $p < 0.001$, comparing Med vs. Large.

© 2015 Macmillan Publishers Limited. All rights reserved

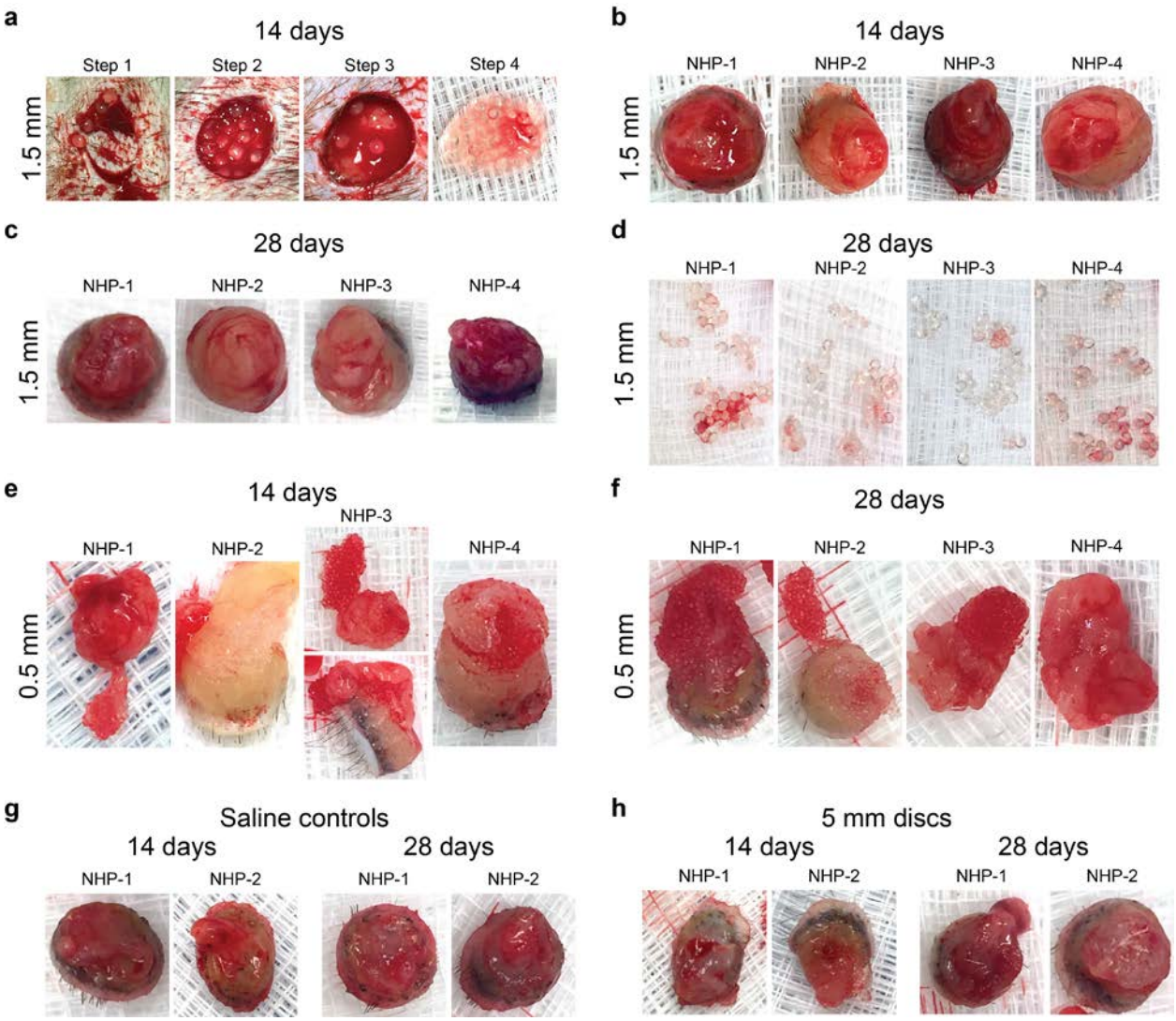

Supplemental Figure S8. Photographs of tissue punches and retrieved alginate spheres from the subcutaneous space of non-human primates (NHPs). Large 1.5 mm-sized spheres of SLG20 hydrogels implanted subcutaneously in the dorsal region of cynomolgus macaques resist fibrosis, while small spheres (0.5 mm sized) and cylinders (4 mm in diameter and 2 mm in height) became fibrosed. After 14 and 28 days 8 mm biopsy punches were used to excise implanted materials along with peripheral host tissue. **a**, 4-step process for tissue/sample retrieval: 1) 8 mm biopsy punch (after which large 1.5 mm spheres freely came out around the still present biopsied tissue core, due to lack of encapsulation), 2) removal of biopsy core (where the majority of the large 1.5 mm spheres were present as a flat (non-encapsulated) layer, which upon removal using forceps (step 3) came out freely, and following subsequent washing in sterile saline to also remove blood from the fresh punch (step 4) appeared clear and easily dissociated away from one another. **b-c**, Clean 1.5 mm sphere-8 mm-biopsy cores (days 14 & 28 post-implant). **d**, Retrieved large SLG20 hydrogels appeared transparent and void of cellular deposition. **e-f,** Free

© 2015 Macmillan Publishers Limited. All rights reserved

DOI: 10.1038/NMAT4290

and non-fibrosed 1.5 mm spheres were separate from any host subcutaneous tissue following a 28-day implantation into the subcutaneous space of n = 4 different non-human primates. 0.5 mm spheres were fibrosed to and embedded in 8 mm-biopsy cores at both 14 and 28 days following implantation into 4 individual primates. **g**, 8 mm punches from NHPs receiving (negative) control subcutaneous saline injections were clean and appeared to be similar to those taken from sites receiving large 1.5 mm SLG20 spheres following both 14 and 28 days (**b-c**), n = 2 NHPs. **h**, 4 mm diameter cylinders were implanted subcutaneously and appear as positive fibrosis controls, as they were heavily embedded in subsequently retrieved biopsy punches, at both 14 and 28 days post-implant (n = 2 NHPs). This finding suggests that just increasing implant size is insufficient to resist foreign body responses, and that a spherical shape is also integral for resisting host fibrosis/rejection.

© 2015 Macmillan Publishers Limited. All rights reserved

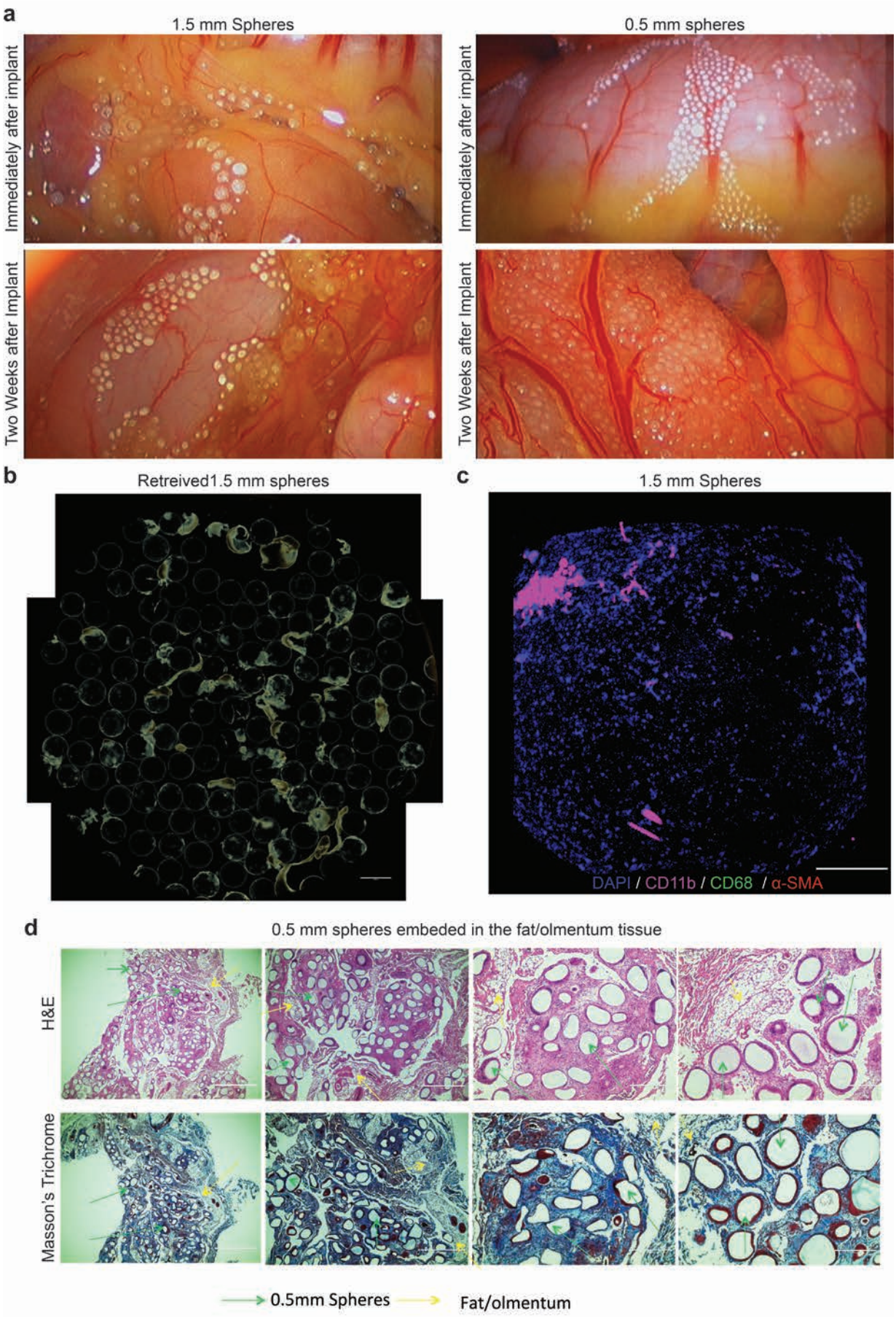

© 2015 Macmillan Publishers Limited. All rights reserved

DOI: 10.1038/NMAT4290

Supplemental Figure S9. Laparoscopic imaging during multiple minimally invasive procedures (one implantation at day 0 and one retrieval at 2 weeks post-implant) for analysis of medium and large SLG20 spheres delivered into the intraperitoneal space of non-human (cynomolgus macaque) monkeys (**a**). Medium (0.5 mm) spheres were almost completely embedded into omental fat tissue, whereas most large (1.5 mm) spheres were free, and often found at the bottom basement of the intraperitoneal cavity. Dark-field phase contrast (scale bar = 2 mm) (**b**) and z-stacked confocal image (**c**) of retrieved spheres following 2 weeks in the intraperitoneal space showing little cellular deposition; In **c** Blue: (DAPI); Green: macrophage (CD68), Magenta (CD11b) and Red: myofibroblast (SMA). Scale bar = 200 μm. (**d**) H&E and Masson's Trichrome histological analysis performed on omental tissues excised 4 weeks post-implantation confirmed the observed largescale adhesion and omental sequestration of medium (0.5 mm) alginate spheres, as shown in the laparoscopic images in panel **a**. Green arrows: embedded medium spheres; Yellow arrows: normal omental fat/adipocyte tissue morphology. (n = 2). 2 left images: 4X, 2 right: 10X.

© 2015 Macmillan Publishers Limited. All rights reserved

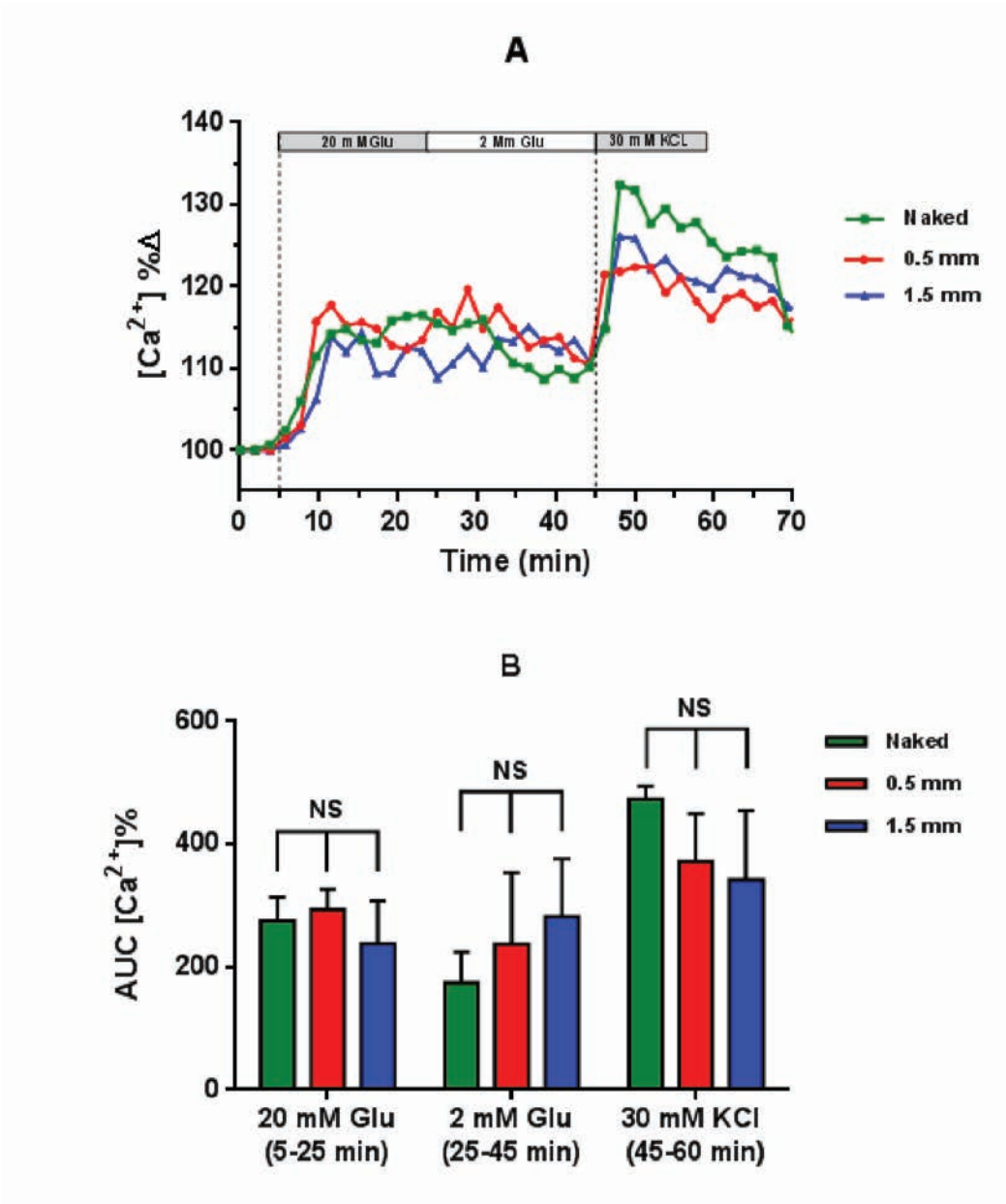

Supplemental Figure S10. Intracellular calcium influx in response to insulin secretagogues. Representative traces of intracellular calcium of single rat islets in response to 20 mM glucose and 30 mM KCl (potassium chloride) stimulus (**A**). Average AUC $[Ca^{2+}]_i$ % of calcium influx in response to 20 mM or 2 mM glucose and 30 mM KCl. Naked n = 59; 0.5 mm n = 49; 1.5 mm n = 43. Mean ± SEM (**B**).

© 2015 Macmillan Publishers Limited. All rights reserved

DOI: 10.1038/NMAT4290

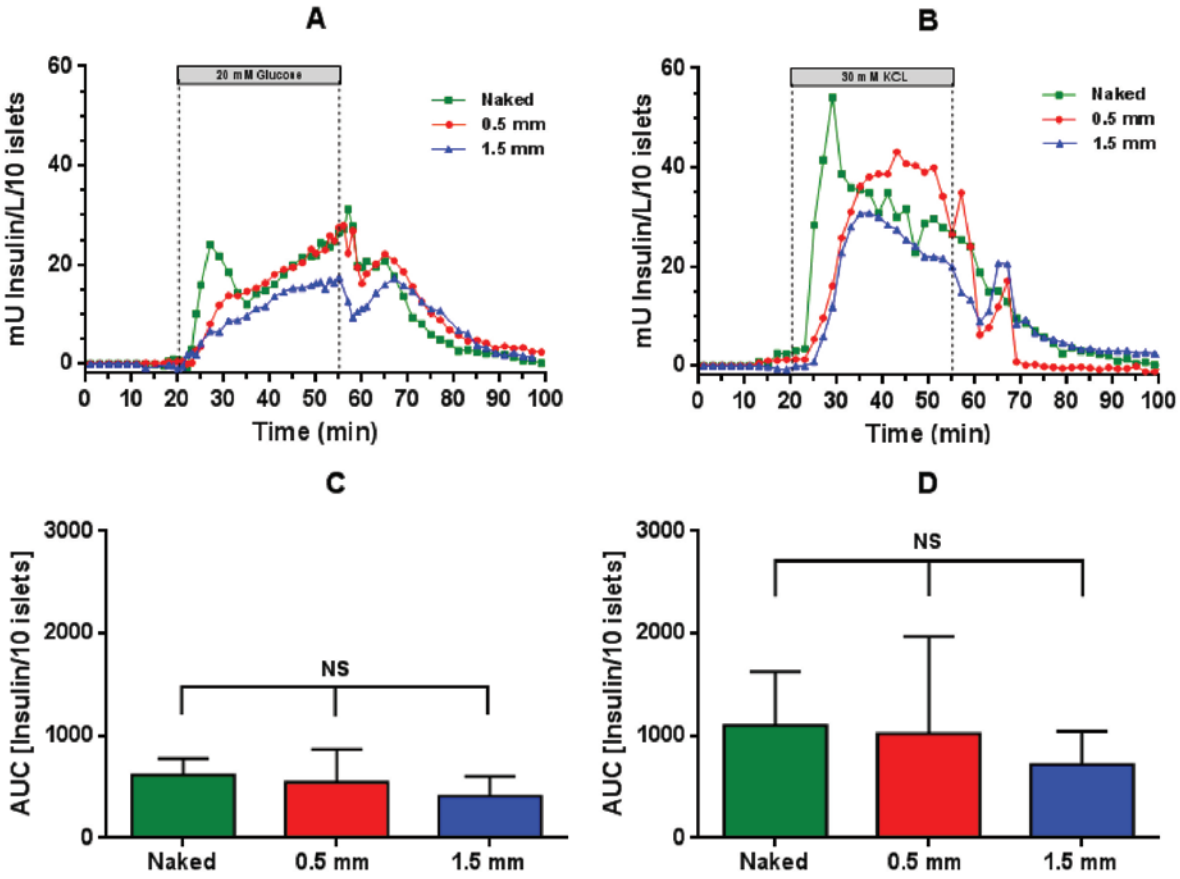

Supplemental Figure S11. Insulin secretion kinetics in response to insulin secretagogues. Average insulin secretion kinetics in response to 20 mM glucose (**A**). Average insulin secretion kinetics in response to 30 mM KCl (potassium chloride) (**B**). Average AUC [Insulin/10 islets] secreted in response to 20 mM glucose (**C**). Average AUC [Insulin/10 islets] secreted in response to 30 mM KCl. (n = 3 groups, each group 50 islets, Mean ± SD) (**D**).

© 2015 Macmillan Publishers Limited. All rights reserved

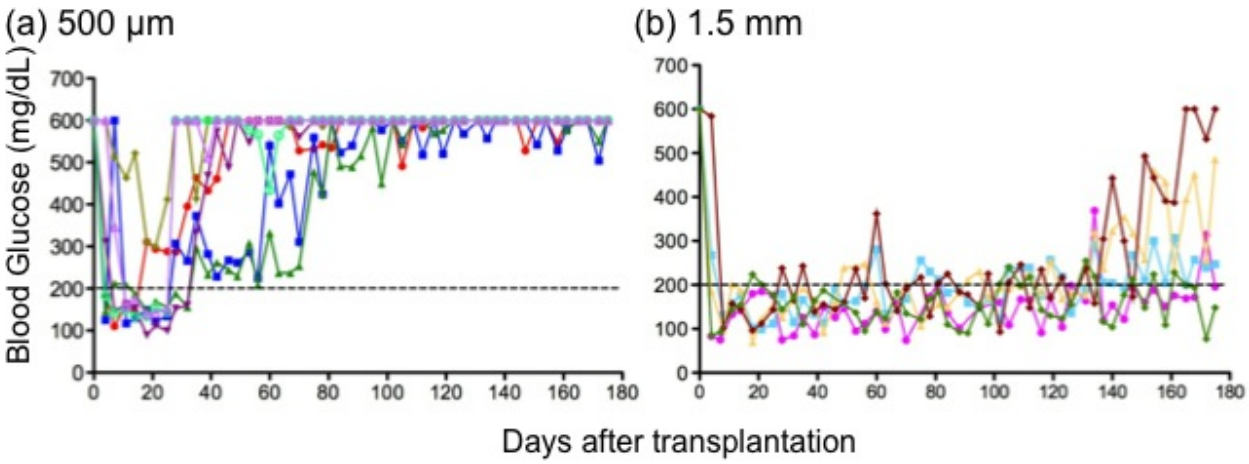

Figure S12. Individual BG correction plots comparing the efficacy of 0.5 mm and 1.5 mm alginate capsules encapsulating rat islets (500 IE's) in curing STZ-induced C57BL/6 diabetic mice. Individual blood glucose curves showing (**a**) only short-lived success with medium 0.5 mm diameter capsules, versus (**b**) prolonged normoglycemia with large 1.5 mm diameter hydrogel alginate capsules. Mean average plots are shown in the main manuscript Figure 4. n = 5-7; repeated twice.

© 2015 Macmillan Publishers Limited. All rights reserved

DOI: 10.1038/NMAT4290

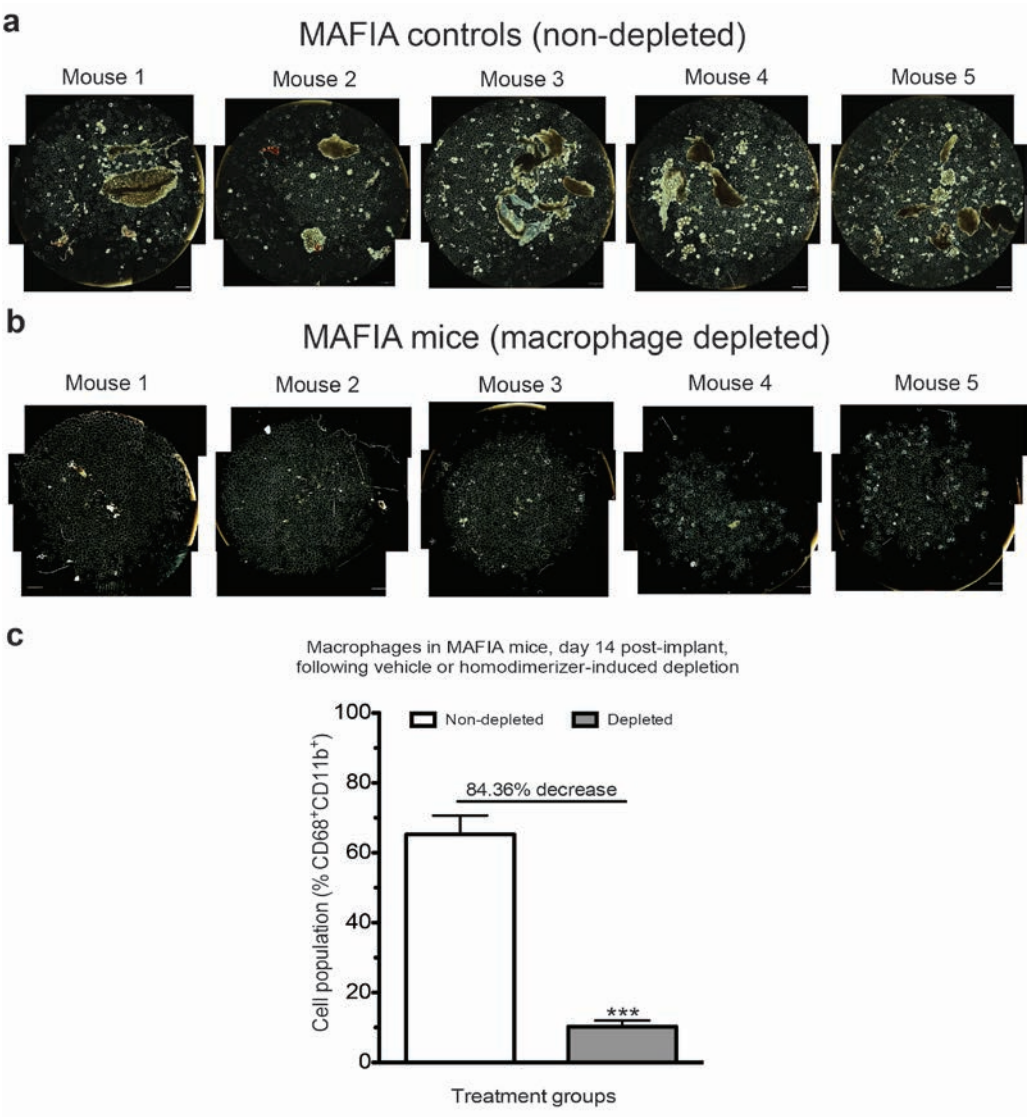

Figure S13. Phase contrast images and FACS data from retrieved Ba-crosslinked SLG20 microspheres of medium (0.5 mm) size 14 days post-intraperitoneal implant into transgenic MAFIA-C57BL/6 mice (non-depleted vs macrophage depleted). Spheres in the control (non-macrophage-depleted) group were heavily clumped and fibrosed (**a**), whereas spheres were clear/translucent, due to a lack of visible fibrotic deposition, in the homodimerizer-induced macrophage depleted treatment group (**b**). The same material volume of hydrogel spheres was implanted into each mouse (n = 5/group) in all cases. Experiments were repeated twice. We achieved significant macrophage depletion (**c**) (~80-90%, mean group decrease = 84.36%) following iv administration of 10 mg/kg of the homodimerizer AP20187 in these mice. Macrophage numbers were knocked down far below peritoneal levels observed in the IP space of SLG20-implanted, non-depleted control MAFIA mice (~65.26% vs ~10.2%).

© 2015 Macmillan Publishers Limited. All rights reserved

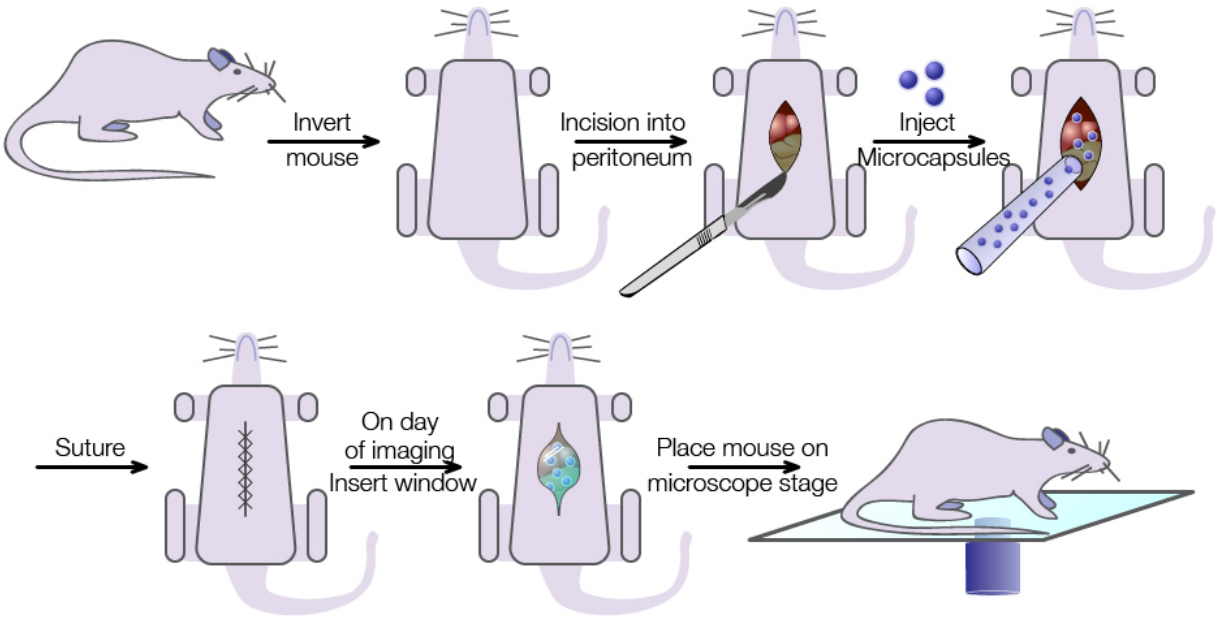

Supplemental Figure S14. Preparation of mice for intravital imaging. The flow of processes involved in preparing mice for implantation with alginate hydrogel spheres, loaded with quantum dots, for *in vivo* intravital fluorescence imaging of macrophage recruitment around and onto implanted spheres.

© 2015 Macmillan Publishers Limited. All rights reserved

DOI: 10.1038/NMAT4290

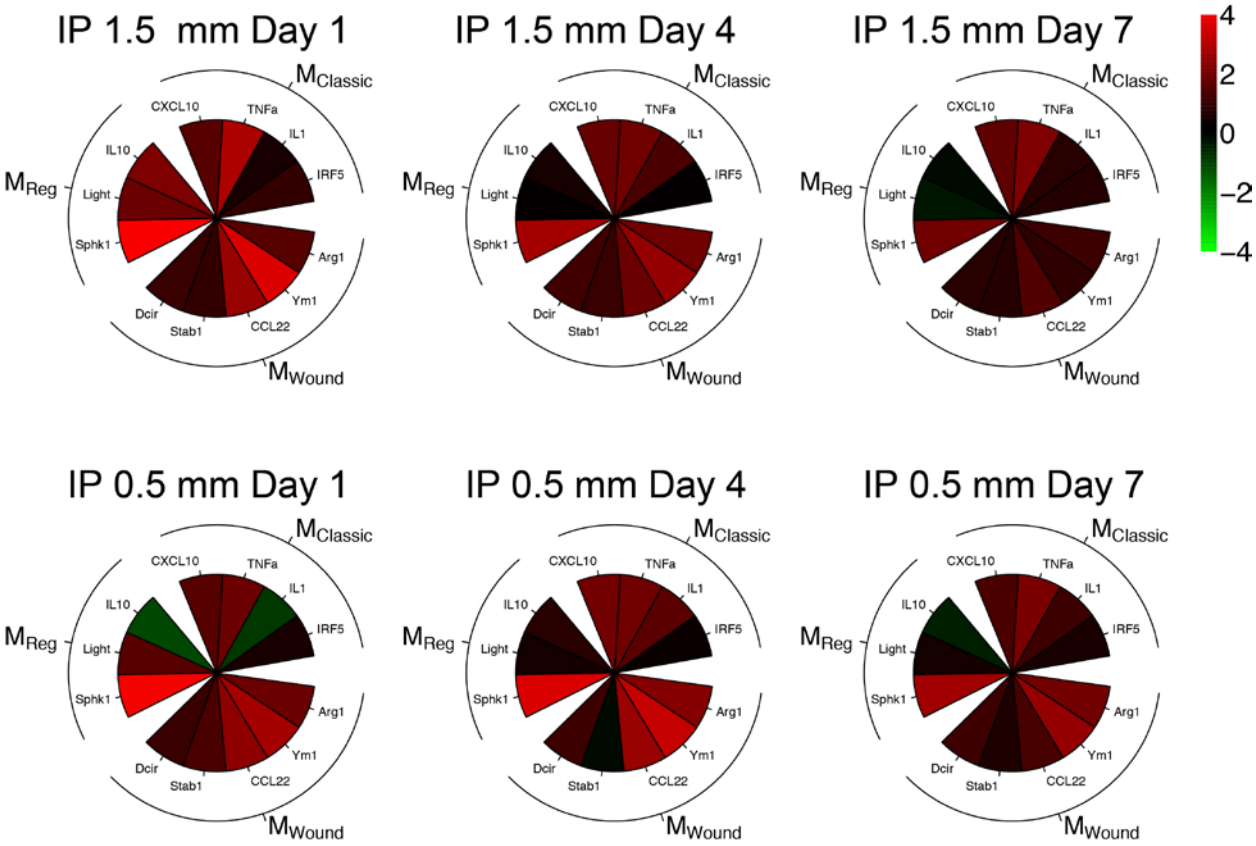

Supplemental Figure S15. Profiling macrophage phenotype shifts in the cells of the intraperitoneal space. NanoString-based analysis for RNA expression of macrophage phenotype markers from cells in the intraperitoneal space extracted (intraperitoneal lavaged) at 1, 4, and 7 days post-implant. Expression is normalized to intraperitoneal cells harvested from mock surgery (PBS-injected) mice, presented on a base 2 logarithmic scale. N=4 mice per treatment. For details of analysis see supplemental methods description.

© 2015 Macmillan Publishers Limited. All rights reserved

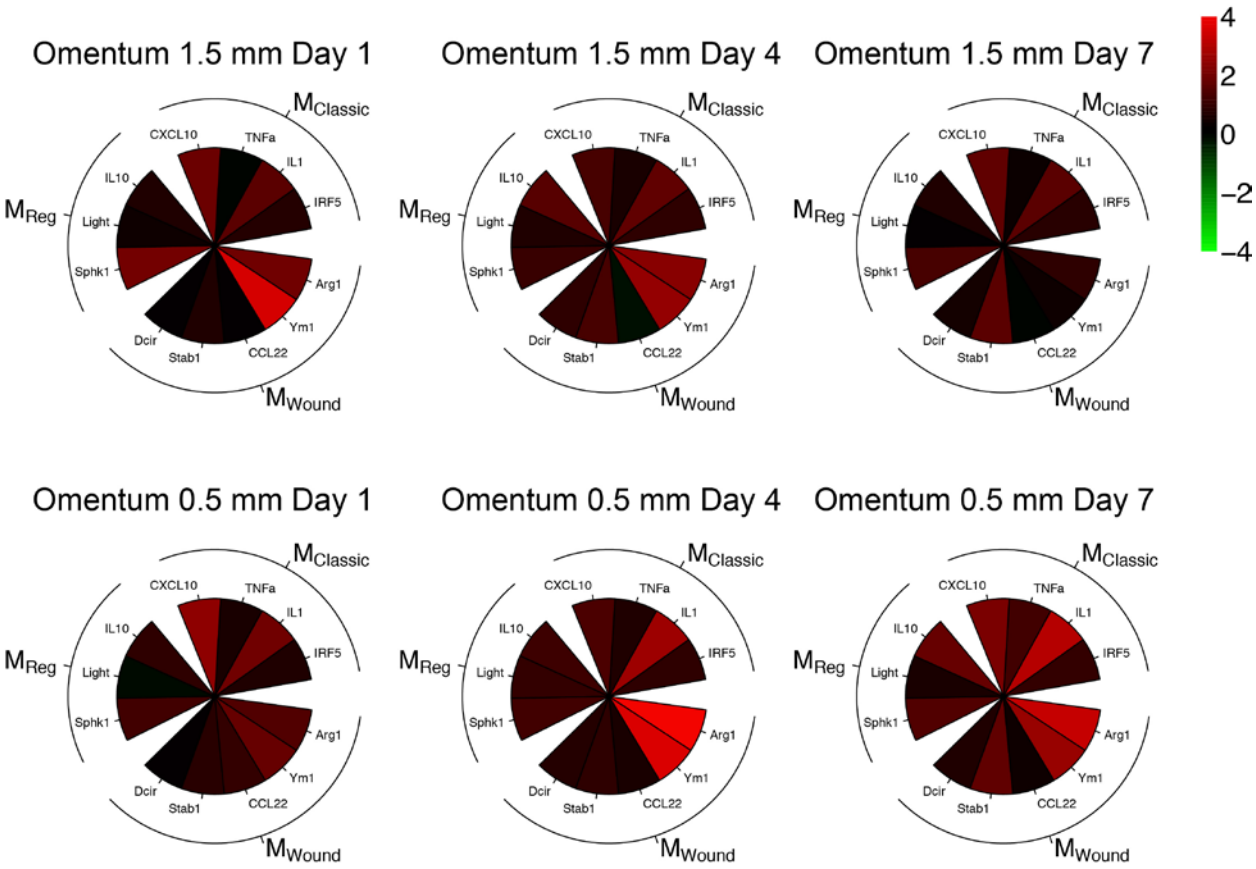

Supplemental Figure S16. Profiling macrophage phenotype shifts in the cell of the peripheral omentum fat tissue. NanoString-based analysis for RNA expression of macrophage phenotype markers from cells in the peripheral fat tissue extracted at 1, 4, and 7 days post-implant. Expression is normalized to fat tissue harvested from mock surgery (PBS-injected) mice, presented on a base 2 logarithmic scale. N=4 mice per treatment. For details of analysis see supplemental methods description.

© 2015 Macmillan Publishers Limited. All rights reserved

DOI: 10.1038/NMAT4290

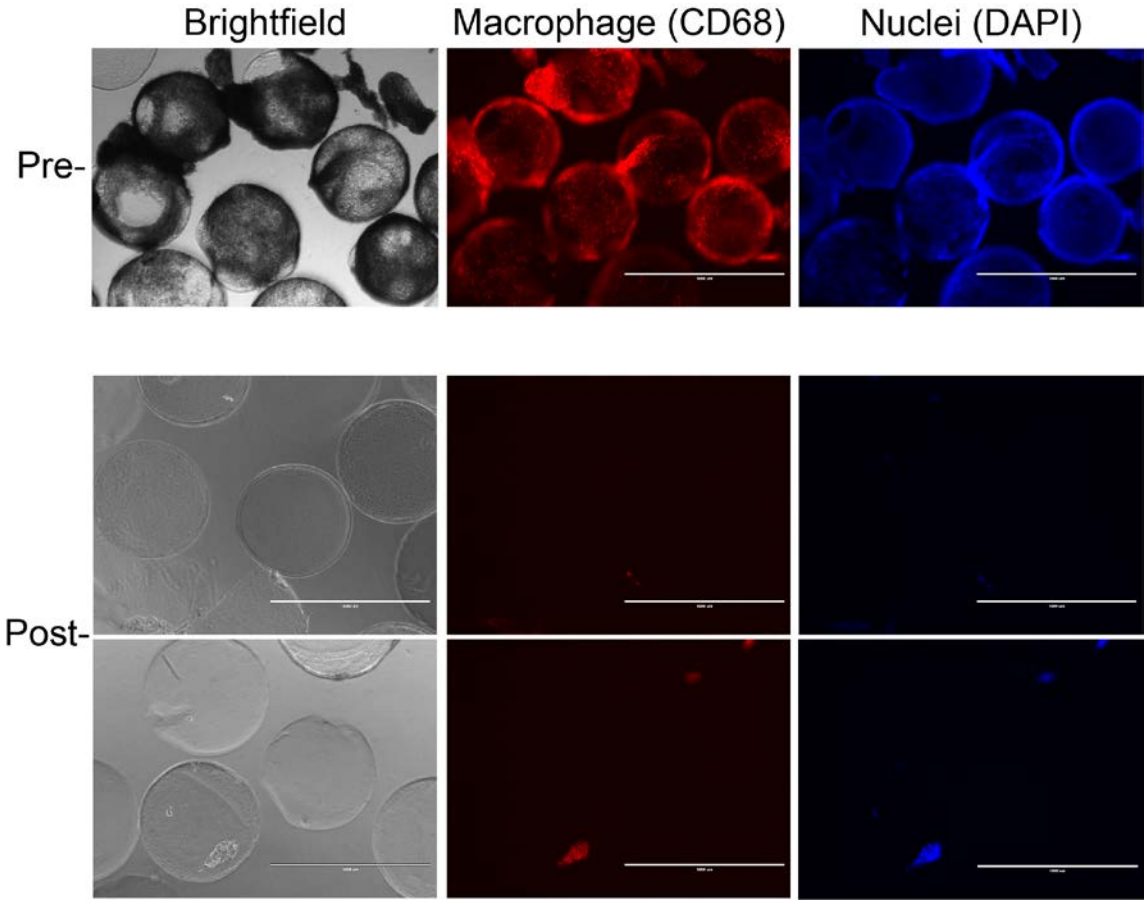

Supplemental Figure S17. Cell dissociation protocol efficacy. To confirm the efficacy of cell removal we did a pilot study were by we immunostained capsules retrieved after a 14-day implantation in the IP space both before (Pre-, top) and after (Post-, bottom) employing our passive cell dissociation protocol (as described in the FACS methods section above). Limited cells remain on capsules after employing this technique, which removed the majority of cells (>90%) adhered to the implanted material.

© 2015 Macmillan Publishers Limited. All rights reserved

5. Supplemental Video Legends:

Supplemental Video V1. Laparoscopic video taken during a minimally invasive procedure (at 2 weeks post-implant) for analysis of medium SLG20 spheres delivered into the intraperitoneal space of non-human (cynomolgus macaque) monkeys. Medium (0.5 mm) spheres were almost completely embedded into omental fat tissue, whereas most large (1.5 mm) spheres were free, and often found at the bottom basement of the intraperitoneal cavity (Supplemental Video V2). An IP lavage with saline at 14 days post implantation was unsuccessful at retrieving 0.5 mm sized spheres due to strong adherence and embedding into the IP host tissue (omentum).

Supplemental Video V2. Laparoscopic video taken during a minimally invasive procedure (at 2 weeks post-implant) for analysis of large SLG20 spheres delivered into the intraperitoneal space of non-human (cynomolgus macaque) monkeys. Medium (0.5 mm) spheres were almost completely embedded into omental fat tissue (Supplemental Video V1), whereas most large (1.5 mm) spheres were free, and often found at the bottom basement of the intraperitoneal cavity. An IP lavage with saline at 14 days post implantation enabled significant retrieval of SLG20 1.5 mm capsules.

Supplemental Video V3. In vivo intravital imaging of macrophage behavior and accumulation at 1 day post-implantation to understand kinetics of host response to SLG20 alginate microspheres of 0.5 mm sizes in diameter, confirms significant macrophage activity and numbers around 0.5 mm sized capsules. N = 3 mice per treatment. Intravital imaging experiments were performed twice.

Supplemental Video V4. In vivo intravital imaging of macrophage behavior and accumulation at 1 day post-implantation to understand kinetics of host response to SLG20 alginate microspheres of 1.5 mm sizes in diameter, confirms a lack of macrophage activity and numbers surrounding 1.5 mm size capsules. N = 3 mice per treatment. Intravital imaging experiments were performed twice.

Supplemental Video V5. In vivo intravital imaging of macrophage behavior and accumulation at 4 day post-implantation to understand kinetics of host response to SLG20 alginate microspheres of 0.5 mm sizes in diameter, confirms significant increases and expansion in macrophage activity and numbers around 0.5 mm sized capsules. N = 3 mice per treatment. Intravital imaging experiments were performed twice.

Supplemental Video V6. In vivo intravital imaging of macrophage behavior and accumulation at 4 day post-implantation to understand kinetics of host response to SLG20 alginate microspheres of 1.5 mm sizes in diameter, confirms a prolonged lack of macrophage activity and numbers surrounding 1.5 mm size capsules. N = 3 mice per treatment. Intravital imaging experiments were performed twice.

Supplemental Video V7. In vivo intravital imaging of macrophage behavior and accumulation at 7 day post-implantation to understand kinetics of host response to SLG20 alginate microspheres of 0.5 mm sizes in diameter, confirms significant and continued increases and expansion in macrophage activity. N = 3 mice per treatment. Intravital imaging experiments were performed twice.

© 2015 Macmillan Publishers Limited. All rights reserved

DOI: 10.1038/NMAT4290

Supplemental Video V8. In vivo intravital imaging of macrophage behavior and accumulation at 7 day post-implantation to understand kinetics of host response to SLG20 alginate microspheres of 1.5 mm sizes in diameter, confirms a lack of macrophage activity and numbers surrounding 1.5 mm size capsules even 7 days post-implantation. N = 3 mice per treatment. Intravital imaging experiments were performed twice.

6. Supplementary References:

1. Morch YA, Donati I, Strand BL, Skjak-Braek G. Effect of Ca2+, Ba2+, and Sr2+ on alginate microbeads. *Biomacromolecules* 2006, **7**(5)**:** 1471-1480.

2. Lacy PE, Kostianovsky M. Method for the isolation of intact islets of Langerhans from the rat pancreas. *Diabetes* 1967, **16**(1)**:** 35-39.

3. Ricordi C, Gray DW, Hering BJ, Kaufman DB, Warnock GL, Kneteman NM*, et al.* Islet isolation assessment in man and large animals. *Acta Diabetol Lat* 1990, **27**(3)**:** 185-195.

4. Adewola AF, Lee D, Harvat T, Mohammed J, Eddington DT, Oberholzer J*, et al.* Microfluidic perifusion and imaging device for multi-parametric islet function assessment. *Biomedical microdevices* 2010, **12**(3)**:** 409-417.

5. Keizer J, Magnus G. ATP-sensitive potassium channel and bursting in the pancreatic beta cell. A theoretical study. *Biophysical journal* 1989, **56**(2)**:** 229-242.

© 2015 Macmillan Publishers Limited. All rights reserved